Nanoscale

REVIEW

View Article Online
View Journal | View Issue

Cite this: *Nanoscale*, 2020, **12**, 7433

Macroscopic two-dimensional monolayer films of gold nanoparticles: fabrication strategies, surface engineering and functional applications

Liping Song,[a] Youju Huang, *[a,b,d] Zhihong Nie *[c] and Tao Chen *[a]

Received 5th November 2019,
Accepted 22nd February 2020

DOI: 10.1039/c9nr09420b

rsc.li/nanoscale

In the last few decades, two-dimensional monolayer films of gold nanoparticles (2D MFGS) have attracted increasing attention in various fields, due to their superior attributes of macroscopic size and accessible fabrication, controllable electromagnetic enhancement, distinctive optical harvesting and electron transport capabilities. This review will focus on the recent progress of 2D monolayer films of gold nanoparticles in construction approaches, surface engineering strategies and functional applications in the optical and electric fields. The research challenges and prospective directions of 2D MFGS are also discussed. This review would promote a better understanding of 2D MFGS and establish a necessary bridge among the multidisciplinary research fields.

1. Introduction

As one of the most widely studied noble metal materials, gold nanoparticles (Au NPs) have attracted tremendous interest in various fields, due to their unique optical and electronic properties.[1,2] Unlike their counterparts including individual Au NPs in solution and bulk materials, Au NP assemblies exhibit unique physical and chemical properties that arise from the synergistic interparticle interactions between the constituent particles.[3–5] Organizing Au NPs into assemblies such as linear Au NP assemblies (1D),[6–9] 2D MFGS[10] and 3D Au NP superstructures[11] with controllable particle spacing and particle

[a]*Key Laboratory of Marine Materials and Related Technologies, Zhejiang Key Laboratory of Marine Materials and Protective Technologies, Ningbo Institute of Material Technology and Engineering, Chinese Academy of Sciences, Ningbo, 315201, China. E-mail: yjhuang@hznu.edu.cn, tao.chen@nimte.ac.cn*
[b]*College of Materials, Chemistry and Chemical Engineering, Hangzhou Normal University, Hangzhou, Zhejiang 311121, China*
[c]*State Key Laboratory of Molecular Engineering of Polymers, Department of Macromolecular Science, Fudan University, Shanghai, 200438, P. R. China. E-mail: znie@fudan.edu.cn*
[d]*National Engineering Research Centre for Advanced Polymer Processing Technology, Key Laboratory of Materials Processing and Mold (Zhengzhou University), Ministry of Education, Zhengzhou University, Zhengzhou 450002, P. R. China*

Liping Song

Liping Song was born in Yichang, China in 1991 and received her Master's degree in applied chemistry from Huazhong Agricultural University in China (2017). She is now a Ph.D. student of the Ningbo Institute of Materials Technology and Engineering, Chinese Academy of Sciences. Her current research is focused on the fabrication, functionalization and application of 2D gold nanoparticle monolayer films.

Youju Huang

Youju Huang obtained his BSc in Polymer Science and Engineering from Anhui University in 2005, and PhD at the University of Science and Technology of China in 2010. He did postdoctoral research from 2010 to 2014 at Nanyang Technological University, Singapore. He joined Ningbo Institute of Materials Technology and Engineering, Chinese Academy of Sciences as an Associate Professor in 2013, and was promoted to Full Professor in 2015. His current research interests focus on the controlled synthesis, macroscopic self-assembly and functional applications of nanoparticles.

arrangement enables the exploration of new applications in various fields including catalysis,[12–15] sensors,[16–18] optoelectronic devices,[19,20] optothermal devices,[21,22] and detection.[23,24] Generally, 1D Au NP assemblies are prepared in solution, leading to the difficulty in yields for the engineering fields.[25–28] Although 3D Au NP superstructures possess numerous advantages, the construction of 3D Au NP superstructures with controllable particle distribution, especially using anisotropic Au NPs, is still challenging.[29–31] In contrast, 2D MFGS display intriguing properties such as good accessibility and stability, transferrable, tuneable plasmon coupling and electromagnetic enhancement.[32–35] Over the past decade, new approaches have been focused on to construct optimized 2D MFGS. Generally, there are three main methods including interfacial assembly,[32,36,37] *in situ* reduction and deposition methods.[38,39] Tremendous efforts have been devoted to interfacial assembly due to the time-saving, easy and simple fabrication procedure, as well as advantages in large area and highly tuneable Au NP distribution of the obtained film. Recently, some exciting interfacial assembly approaches have been developed, which can solve the problems of films such as poor mechanical strength and low conductivity.[40] They also result in some distinctive or enhanced properties of 2D MFGS, which is promising in the combination of flexible polymer substrates for wearable electrical devices.[41] In consequence, the rise of 2D MFGS prompted a rich variety of new technologies in sensing and detection,[10,42] and optical and electronic devices.[43–47]

2. General consideration

Although some reviews about the self-assembly of Au NPs in solution have been reported, there is still no reported review primarily on 2D MFGS.[48,49] In this review, we provide an in-depth summary of 2D MFGS focusing on the various interfacial self-assembly methods, and the surface engineering achieved *via* combining with functional materials such as functional small molecules, smart polymers and bio-substances. We also outline key challenges and the prospective directions of 2D MFGS for future research (Fig. 1).

3. The construction of 2D MFGS

The high accessibility, stability and controllable physical properties[40,50] make the 2D free-standing MFGS more applicable. It is, therefore, particularly important to construct 2D MFGS with required functions for different fields. The ideal approach for preparing 2D MFGS should satisfy the following points: (1) from the standpoint of fundamental research and real practical applications, the method should be low-cost and exhibit high-reproducibility, reliable scalability and ignorable environmental toxicity. (2) The construction approaches of 2D MFGS should be tailored to meet the materials requirements in different fields. For instance, in the current research of SERS detection, repeatability is also a key technology area to be focused on besides the improvement of sensitivity. Therefore, the regularity of the arrangement of nanoparticles in 2D MFGS is of great importance, which provides the coupling of hot spots for enhancing the stability and reliability of surface-enhanced Raman scattering (SERS) detection. (3) The prepared 2D MFGS should possess good physical and chemical properties (conductivity, transferability, stability, large specific surface area, *etc.*) for on-demand 2D MFGS based devices.[51–53] Interfacial self-assembly is a spontaneous assembly process in

Zhihong Nie

Zhihong Nie is a Distinguished Professor in the Department of Macromolecular Science at Fudan University, China. Prior to his current appointment, he was a Tenured Associate Professor in the Department of Chemistry and Biochemistry at the University of Maryland, College Park. Dr Nie received his PhD degree in Polymer Materials and Chemistry from the University of Toronto in 2008. He then worked as an NSERC Postdoctoral Fellow in George M. Whitesides' group at Harvard University (2008–2010). He was the recipient of a number of awards including the CMNS Outstanding Junior Faculty Award (2014), 3 M Non-tenured Faculty Award (2013–2015), ACS PRF Doctoral New Investigator Award (2013), NSF CAREER Award (2012), etc. *His research interests include polymer and nanoparticle self-assembly, cancer theranostics, programmable soft materials, and microfluidics.*

Tao Chen

Tao Chen received his PhD degree in polymer chemistry and physics from Zhejiang University (Prof. Li Wang group) in 2006. After his postdoctoral training in the Department of Chemistry at the University of Warwick (Prof. Stefan A.F. Bon group), he joined Prof. Stefan Zauscher's group at Duke University as a research scientist. He then moved back to Europe as an Alexander von Humboldt Research Fellow hosted by Prof. Rainer Jordan at Technische Universitat Dresden, Germany. Since 2012 he has been a full professor at Ningbo Institute of Materials Technology and Engineering, Chinese Academy of Sciences upon being awarded with the Thousand Young Talents Program by the Chinese Central Government. His research interests include smart polymers and their hybrid systems with applications as shape memory polymers and actuators, and in chemical sensing.

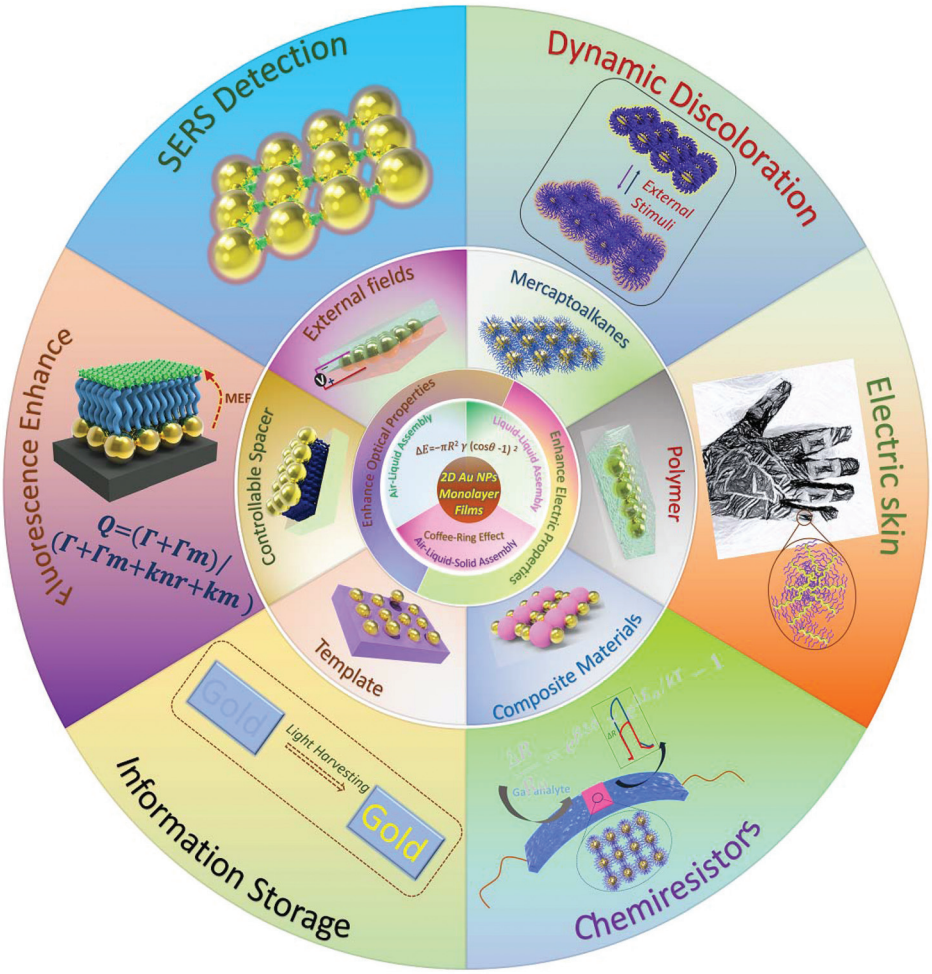

Fig. 1 Schematic overview of this review including the fabrication approaches, surface engineering strategies and mainly optical and electric applications of 2D MFGS.

a restricted two-dimensional plane, which can help prepare ordered structures in the microscopic scale with desired functions.[54] According to the three basic states (phases) of matter, the 2D interface can be divided into gas–liquid, liquid–liquid and gas–liquid–solid interfaces for constructing of 2D MFGS.

3.1 Air–liquid interface assembly

The assembly of gold nanoparticles at air–water interfaces into microscopic 2D colloidal crystals was firstly exploited by Pieranski.[55] The gas–liquid interfacial assembly of nanoparticles is a process of adsorption.[56,57] Thermodynamically, the Gibbs free energy (ΔE) of gold nanoparticles at the air–water interface can be calculated as follows:[58]

$$\Delta E = -\pi R^2 \gamma_{\mathrm{air/water}} (\cos\theta - 1)^2 \quad (1)$$

where θ, R and γ are the contact angle of Au NPs in aqueous solution, particle radius and interfacial tension, respectively.

Apparently, ΔE is always negative and the transferring of Au NPs to the air–water interface is a process of reducing Gibbs free energy regardless of the hydrophobicity of Au NPs. That is, in view of thermodynamics, it is a spontaneous procedure to transfer Au NPs from solution to the interface (Fig. 2).[59,60] However, it is always difficult to achieve spontaneous interfacial assembly without any extra force. Universally acknowledged, the kinetics inhibits particle adsorption due to the high sorption potential barrier (G).[60,61] In order to achieve assembling of Au NPs at the air–water interface, additional impetus was often added into the system. Previous experiments and a great quantity of simulation about interfacial assembly revealed that adding electrolytes,[62–65] performing hydrophobic modification[66–70] and using surface active solvents could strongly facilitate the decrease of the sorption barrier in the assemblies of Au NPs. Reducing the surface charge density is the main principle of electrolytes inducing the assembly of Au NPs. In early days, the assemblies were acquired by adding strong electrolytes to the colloidal solution.[62] This method is very effective for rapid assembly; however, a slight change of the electrolyte concentration usually results in the bulk coagulation of the colloids, which

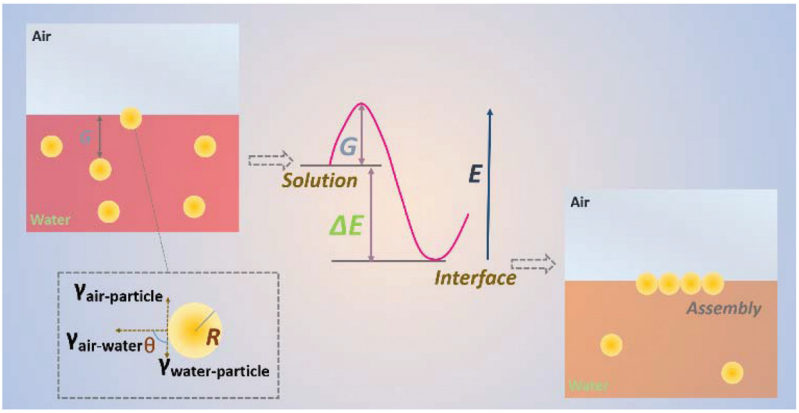

Fig. 2 Diagrammatic sketch of thermodynamic and kinetic changes in the process of 2D GNMS formation at the air–liquid interface. During this process, the reducing Gibbs free energy (ΔE) implied that 2D GNMS formation is a thermodynamically spontaneous process. However, it kinetically inhibits particle adsorption (G).

makes this approach uncontrollable.[63] With the development of this assembly strategy, replacing strong electrolytes with weak electrolytes is the current predominant direction.

As shown in Fig. 3a, Deng's group[64] achieved the assembly of Au spheres at the air–liquid interface by using a weak electrolyte (formic acid). Better control of the decrease of the particle surface charge density would prevent the coagulation of the colloids effectively. Additionally, the generation of a proton gradient achieves vertical segregation of Au spheres with different sizes. Nevertheless, the sophisticated operation and precise concentration restricted further advancement of this method. Alternatively, the hydrophobic modification of gold particles also plays an important role in decreasing the surface charge density for air–liquid self-assembly. The assembly mechanism of Au NPs *via* hydrophobic modification is similar to the addition of electrolytes. More importantly, the incom-

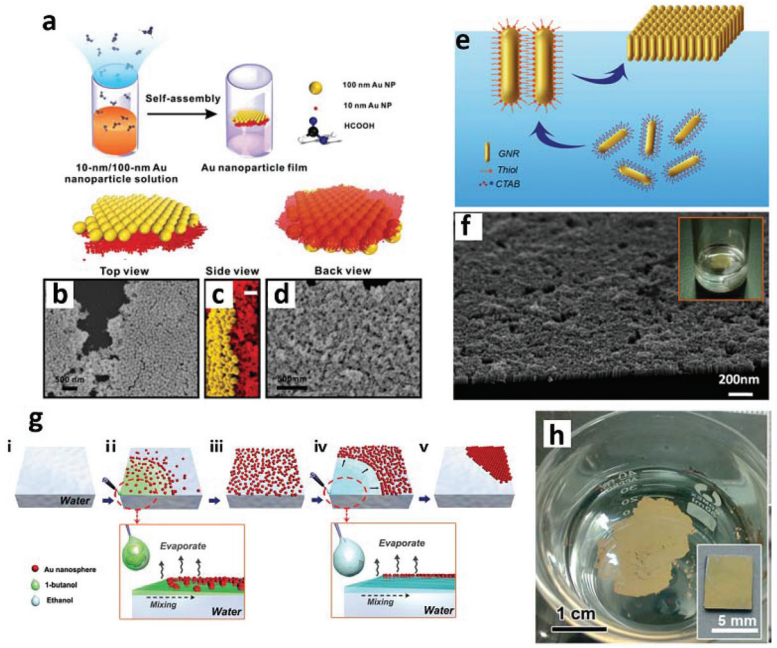

Fig. 3 Electrolytes induced assembly of Au NPs:[64] (a) Schematic illustrations of the fabrication of Au NS films through weak electrolyte (formic acid vapor) induced assembly at the water–air interface; (b–d) SEM images of the size-segregated double-layered Au NS films. Hydrophobic modification (thiol) induced assembly of Au NRs at the air–water interface:[66] (e) schematic illustrations of the fabrication of vertical Au NR films; (f) SEM images and physical photographs of the prepared vertical Au NR monolayer. Surface active agents induced the assembly of Au NSs at the air–water interface:[74] (g) schematic of the fabrication of a Au NS array film by a capillary gradient-induced self-assembly at air/water interfaces. The assembly process was achieved in two steps: (1) pre-assembly. PDDA-coated Au NSs pre-assembled into Au NS chains; (2) extrusion. The Au NS chains were extruded into dense Au NS arrays by ethanol; and (h) a photograph of the macroscopic Au NS array films.

patibility between the Au NP surface and surrounding solvent enables the NPs to be readily transferred to the interface for reducing the surface energy.[70] Wei *et al.* (Fig. 3b) achieved the self-assembly of Au NRs into a monolayer vertical array at the air–water interface by modifying the Au NRs with mercapto alkane (1-dodecanthiol).[54] In addition, the assembly of the hydrophobic molecule modified Au NPs *via* the Langmuir–Blodgett[71,72] approach is an effective strategy to achieve macroscopic assembly of Au NPs.[73] Alternatively, the addition of active solvent is another efficient approach to achieve dense assemblies of Au NPs at the air–water interface. Generally, the active solvent often causes an abrupt change of the surface tension of Au NPs. Unconventionally, Li's group[74] acquired a dense monolayer of Au NPs by using volatile organic solvents (ethanol) (Fig. 3c). Without adding ethanol, the dipole–dipole interactions and electrostatic repulsions between Au NPs resulted in random, non-close-packed NP assemblies at the air–water interface. In contrast, the addition of ethanol effectively facilitates the formation of dense and macroscopic 2D MFGS.

3.2 Liquid–liquid interface assembly

Compared with air–liquid assembly, liquid–liquid assembly with higher anti-interference capacity makes it easier to obtain dense and macroscopic MFGS. Generally, the key elements of liquid–liquid assembly are as follows: (1) two immiscible liquid phases with large difference in surface tension. One shows good dispersion of Au NPs, and is identified as the water phase. Au NPs are usually dispersed in the water phase because of their initial synthesis in the water phase[75,76] with soluble surface capping agents.[77] The other is the oil phase, which has a wide range of choices, such as chloroform,[78] dichloromethane,[79,80] toluene,[81–83] hexane,[84,85] cyclohexane,[86] heptane,[87,88] pentanol[89] and so on. Generally, hexane is extensively used, due to its strong volatility, nonpolarity, low density and stability, as shown in Fig. 4a. (2) Triggers to induce instability of Au NPs in solution and enable energy transfer to the interface. Adding some solvent with a low dielectric constant has been the most commonly used strategy to compel Au NPs to the interface. As with air–liquid interfacial assembly, the acting solvent was effective at decreasing the surface charge of Au NPs. Furthermore, weakening the electrostatic repulsion between the Au NPs and interface immediately causes the assembly.[59] For instance, Jiang's group[17] prepared Au NP monolayers by adding ethanol to reduce the surface charge of Au NPs without any assistance from molecular ligands (Fig. 4a–e). Additionally, physical promoting force such as shaking or vigorous mixing has been implemented to increase the assembly efficiency.[78,90–93] For example, Mohan and co-workers[95] reported an effective approach to improve assembly efficiency by shaking the two-phase mixture (Fig. 4f–h).

Nevertheless, the fabrication of 2D MFGS with a large area, controllable gaps between adjusted particles, good stability, and high particle close-packing is still a significant challenge. In addition, it is often difficult to assemble large sized Au NPs into monolayers. As shown in Fig. 5a, the steric repulsion coexists with long-range vdW attraction between Au NPs and changes with the spacing between Au NPs according to the DLVO theory.[96,97] For small Au NPs (d < 10 nm), the particle curvature is high enough for significant chain mobility, which is favourable for controllable Au NP assembly.[98] However, the

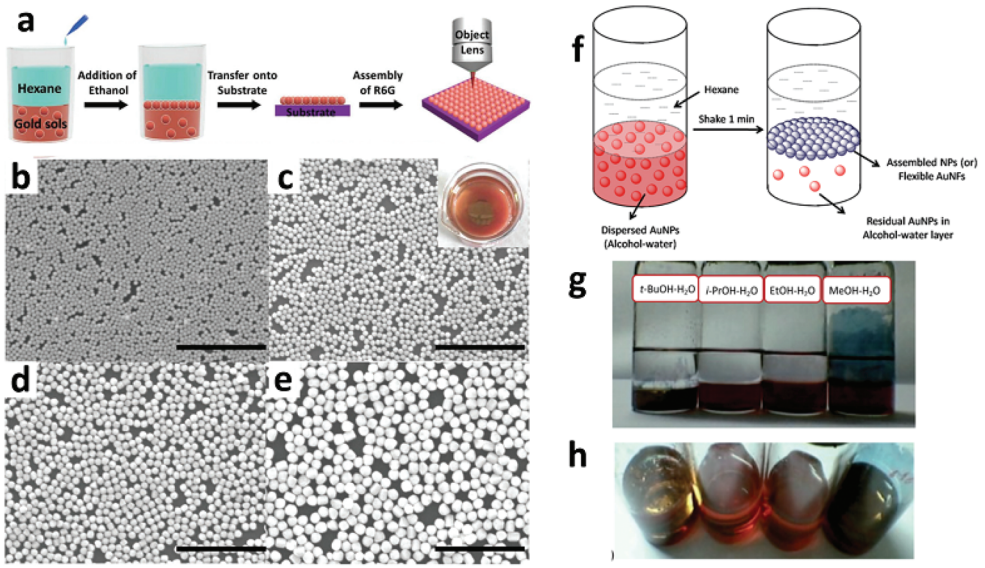

Fig. 4 Two typical examples of Au NPs assembled at the liquid–liquid interface: (1) Au NSs assembled at the hexane–water interface by adding a promoting agent:[17] (a) schematic illustrations of Au NSs assembled at the hexane–water interface by adding ethanol in the water phase; Au NS films with different Au NS sizes: (b) 30 nm, (c) 60 nm, (d) 90 nm, and (e) 120 nm. The scale bar is 1 μm. (2) Au NSs assembled at the hexane–water interface by shaking:[92] (f) schematic illustrations of Au NSs assembled at the hexane–water interface by shaking; the influence of alcohols on the assembling effect: (g) side view; and (h) top view.

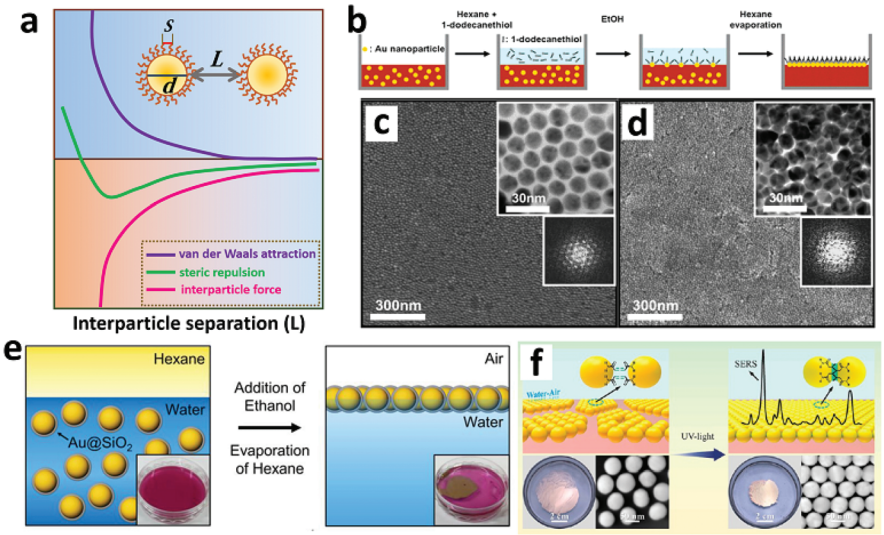

Fig. 5 (a) Description of forces between two Au NPs. The parameter *s*, *d* and *L* represent separation between chains coated on Au NPs, the diameter of Au NPs and the spacing of adjacent Au NPs. Obtaining close-packed Au NS monolayers by inducing long-chain alkanethiols in the oil phase (hexane) during the liquid–liquid assembly process (b).[103] The Au NSs assembled under different amounts of 1-dodecanethiol: (c) moderate amount and excess amount (d); (e) schematic representation of the fabrication of the Au NS monolayer with an ultra-small void nanogap: Au@SiO_2 assembled at the water–oil interface followed by etching of the SiO_2 shell to obtain the Au NS monolayer ultra-small void nanogap.[5] (f) Schematic illustration of shrinkable Au NP monolayer films induced by interfacial cross-linking at the water–oil interface.[106]

surfactants usually induced assembly into close-packed domains for larger Au NPs due to low chain mobility. As a result, uncontrollable assemblies and multilayers usually appear.

In recent years, much effort has been devoted to improve the properties of Au NP assemblies.[99–102] The hydrophobic modification of gold particles is an effective approach for optimizing the uniformity of Au NP assemblies. Typically, as shown in Fig. 5b–d, Park and co-workers[103] obtained dense close-packed Au NP films by utilizing long-chain alkanethiols coated on Au NPs. By forming organic layers around Au NPs, the residual electrostatic repulsive force was converted into a van der Waals interaction[88] to further decrease the surface charge density of Au NPs.[94] It is noteworthy that the concentration of alkanethiols should be adjusted felicitously to avoid the formation of multilayers. Hallinan's group reported the preparation of 2D MFGS *via* interfacial ligand exchange induced interfacial transfer (from water/oil to water/air) of Au NP films.[104] They also theoretically confirmed that the interfacial energy was responsible for the particular phase transfer. Additionally, the spontaneous rearrangement of Au NPs at the water/air interface aimed to eliminate the free volume and this was good for acquiring uniform 2D MFGS. Although the coating of long-chain alkanethiols is a good strategy to achieve close-packed 2D MFGS at the liquid–liquid interface, especially for small Au NPs,[105] the high stability and controllable interparticle spacing of 2D MFGS still posed a challenge. The sacrificial template method is a good alternative to gain a controllable gap between adjusted particles of Au NP films. Kang's group[5] fabricated a Au NS monolayer by assembling gold–silica core–shell nanoparticles at a water–oil interface. Subsequently, the Au NS monolayer with a controllable gap was obtained by etching a silica shell in an alkaline environment (Fig. 5e). Additionally, the macroscopic Au NP film with a controllable gap and good mechanical stability is in line with the current demands.[73] Chemical crosslinking of Au NPs is a good means to achieve good mechanical stability and adjustable gaps without affecting the surface properties or activities of 2D MFGS.[93] Inspired by previous work on utilizing covalently bonded Au NPs to obtain a free-standing monolayer,[90] our group[3] further promoted this strategy by applying light-controlled chemical crosslinking of molecules (acrylamide) (Fig. 5f). Initially, amino (acrylamide) bound Au NPs were pre-assembled into a 2D monolayer at a water–oil interface by adding ethanol in water. Then the light-controlled chemical crosslinking between acrylamide molecules was accompanied by the shrinkage of 2D MFGS, which implied further close-packing of the Au NPs. The obtained film was mechanically stable, which greatly facilitates the application of 2D MFGS.

3.3 Air–liquid–solid interface assembly

When a drop of NP solution is spread on a solid substrate, the evaporation of the solvent is accompanied by organization of NPs into monolayers induced by long-range dispersion forces.[107] That is why air–liquid–solid interfacial assembly is also named "droplet evaporation induced assembly". This approach has been intensively investigated due to its cost-effectiveness,[108] convenience,[109,110] and wide applicability to various functional nanomaterials.[109] The air–liquid–solid interfacial assembly has less limitations but is difficult to manipulate compared with other interfacial assembly methods. In detail, the solvent should have good dispersion

for Au NPs and certain volatility. However, it is hard to obtain complete 2D MFGS *via* air–liquid–solid interfacial assembly due to the so-called "coffee-ring effect". During the process of solvent evaporation, NPs tend to accumulate at the edge of pinned drops resulting from the faster solvent evaporation at the contact line, which is commonly known as the "coffee-ring effect".[111] Despite some previous work reporting that the existence of the coffee-ring is favourable for enriching analytes,[112,113] the non-uniformity of 2D MFGS has become a barrier to the application of Au NP films.[114] It is remarkable that there is some reported work with practical significance that the periodic particle assemblies can be obtained *via* subphase surface assisted drying-driven assembly.[115] However, there are still some limitations such as the complicated assembly procedure and requirement of a substrate. Recently, great efforts have been devoted to suppress the coffee-ring effect and are commonly divided into three strategies: (1) reducing the capillary force from the center to the edge of the droplet. The faster solvent evaporation at the contact line drives the migration of Au NPs. Therefore, weakening the capillary flow is an efficient strategy to suppress the coffee-ring effect. Many studies have been reported to weaken the capillary flow. For instance, one good method is employing a cold substrate to weaken the capillary flow.[114] In addition, the shape of the NPs played an important role in the final pattern of assemblies.[119] Wang's group[120] reported that Au NPs with different shapes showed great divergence in the final assembled morphologies (Fig. 6a). Moreover, adjusting the size of the droplet is another efficient method to suppress the coffee-ring effect. When the size of the droplet was relatively small, the droplet evaporated rapidly and there was not enough time for transferring the solute to the edge. Wong and co-workers[121] found that the coffee-ring effect gradually became obvious with the increased size of the droplet (Fig. 6b). Additionally, enhancing the interaction between Au NPs was also propitious to weaken the capillary flow. (2) Increasing Marangoni flow. The Marangoni effect refers to a phenomenon of mass shift due to the gradient of tension between two liquid interfaces with different surface tensions, and was found by an Italian physicist, Marangoni.[122] The nonuniform evaporation of the pinned droplet is the immediate cause of the coffee-ring effect. Nevertheless, the Marangoni flow created a flow gradient (such as surface tension, temperature, or concentration) from the center to the edge, which endowed NPs with a kind of force to pull them to the marginal of drops. As a result, NPs recursively flowed in the droplet and the coffee-ring effect was efficiently suppressed. For instance, exposing the NP droplet to vapors of miscible, volatile, low surface tension liquids (ethanol, methanol, and isopropyl alcohol) is an extremely effective strategy to achieve Marangoni flow.[123] In addition, adding a surfactant to create a concentration gradient is another efficient approach to engender Marangoni flow for suppressing the coffee-ring effect. Chu's group[118] reported that the droplet of Au NRs modified with MUDOL ((11-mercaptoundecyl)hexa(ethylene glycol)) enormously attenuated the coffee-ring effect, as shown in Fig. 6c. (3) Sliding of the three phase contact line (TCL). Pinning of the three-phase contact line is one of the necessary parameters for forming a coffee ring during droplet evaporation.[124] Thus, the TCL would move with the decreased size of the droplet, which compels NP deposition on edges and the center. This is an efficient approach to suppress the coffee-ring effect (Fig. 7a).[125–127] For instance, regulating the hydrophobi-

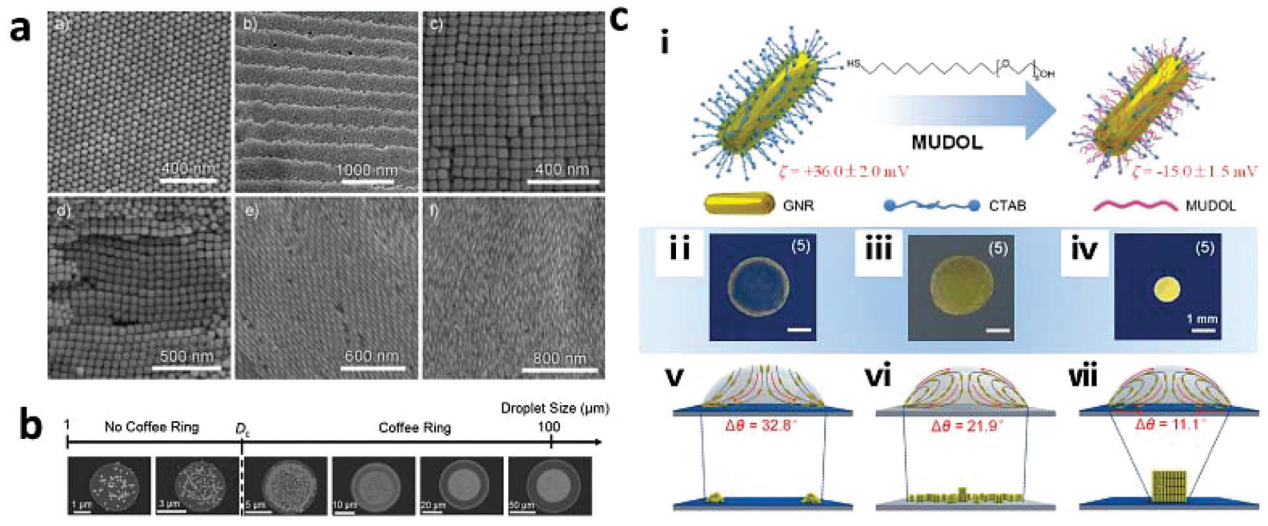

Fig. 6 (a) The ordered assemblies of various shapes of Au NPs;[116] (b) the influence of droplet size on the coffee-ring effect: different nanoparticle droplets with diameters ranging from 3 to 100 μm;[117] (c) generating Marangoni flow for suppressing the coffee-ring effect by regulating the surface properties of the Au NRs:[118] (i) schematic illustration of exchanging the CTAB-AuNRs with MUDOL molecule coated Au NRs; (ii–iv) top views of different Au NR deposition behaviors during evaporation: (ii) CTAB-Au NRs on Si/SiO_2, (iii) MUDOL-Au NRs on Si, and (iv) MUDOL-Au NRs on Si/SiO_2; (v–vii) schematic illustration of the flowing route of different Au NRs: (v) CTAB-Au NRs on Si/SiO_2, (vi) MUDOL-Au NRs on Si, and (vii) MUDOL-Au NRs on Si/SiO_2.

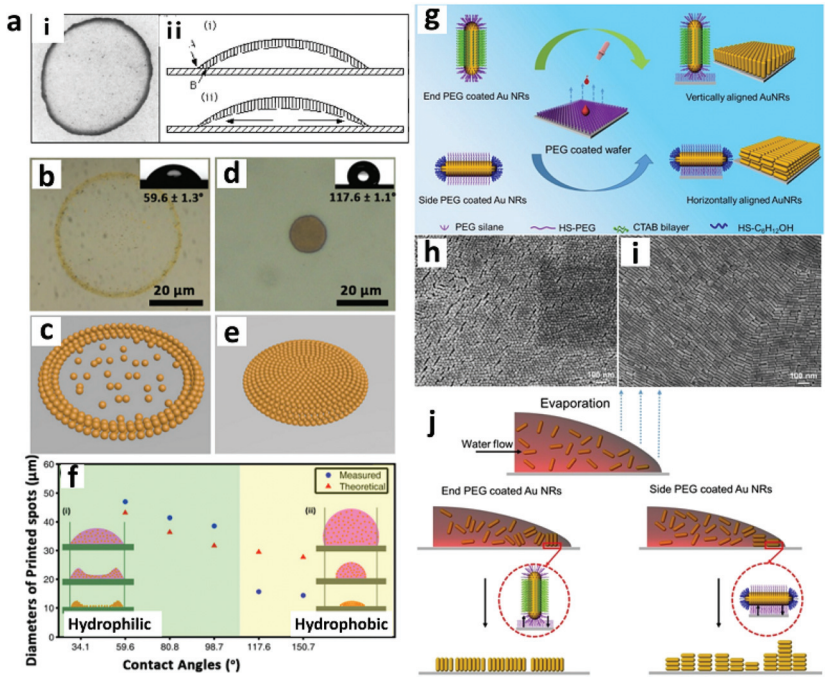

Fig. 7 (a) Schematic illustration of TCL sliding:[127] (i) a photograph of a dried coffee drop; (ii) schematic illustration of pinning TCL (top) and sliding TCL (down); (b–f) adjusting the hydrophobicity of the substrate:[129] optical images (b and d) and corresponding schematic illustration (c and e) of Au NP droplets on the substrate with distinct hydrophobicity; (f) the theoretical and measured values of the size of the Au NP droplets on the substrate with different hydrophobicities; (g–j) suppressing the coffee-ring effect by manipulating the affinities between Au NRs and the substrate:[130] (g) schematic illustration of the preparation of aligned Au NRs on the modified substrate; SEM images of the vertically (h) and horizontally (i) aligned Au NR arrays; and (j) schematic illustration of the self-assembly process and the force between Au NRs and the substrate.

city of the droplet can control the final depositing morphologies.[128] As shown in Fig. 7b–f, Song's group[129] achieved homogeneous distribution of Au NPs during the droplet drying process by controlling the wettability of the substrates. Additionally, enhancing the interaction between the Au NPs and substrate is another efficient approach to suppress the coffee-ring effect. Our group fabricated a directional alignment of Au NRs on a Si substrate *via* adjusting the coordination between the Au NRs and substrate (Fig. 7g–j).[130] Generally, Au NRs are selectively functionalized with two thiol molecules with different properties. As a result, assemblies of Au NRs presented anisotropic orientations on a PEGylated substrate through the polymeric affinity interaction. During the process of assembly, the interaction between the Au NR portion and PEGylated substrate efficiently restricted the droplet capillary flow with TCL depinning. The asymmetric interaction with the substrate induced macroscopic anisotropic assembly of Au NRs with a nearly 100% orientation.

3.4 Other approaches for constructing 2D MFGS

Although interfacial assembly has been the major approach for constructing 2D MFGS, there are still other ways to obtain 2D MFGS for particular applications. For example, electrophoretic deposition has been a direct approach for obtaining macroscopic 2D MFGS. Compared to other methods, it possesses many advantages such as high preparation efficiency and low selectivity for the morphologies and size of Au NPs.[131] Zhang and co-workers reported their efficient approach for preparing 2D MFGS by electrophoretic deposition of Au NPs on patterned and transparent conductive substrates (Fig. 8a).[132] Due to the pretreatment of a patterned substrate, the Au NPs showed high selectivity and high uniformity on the substrate (Fig. 8b and c). Additionally, *in situ* reduction of Au NPs during the preparation of 2D MFGS is another effective method.[133,134] Although it is usually difficult to obtain 2D MFGS with highly uniform particle size and morphologies, this method often shows distinctive properties such as high stability and mechanical strength. For instance, our group presented the construction of biofriendly and regenerable 2D MFGS *via in situ* reduction of Au NPs cross-linked with polydopamine (Fig. 8d).[135]

4. The functionalization of 2D MFGS

Although various methods for constructing 2D MFGS are quite mature, it is usually difficult to apply the obtained films without surface modifications for further applications. There are five main reasons: (1) environmental toxicity. Most interfacial assembly processes of Au NPs were conducted with environment polluting organic solvents (chloroform, dichloromethane, and toluene). (2) Interference immunity. The interface assembly process is easily interfered with by ambient

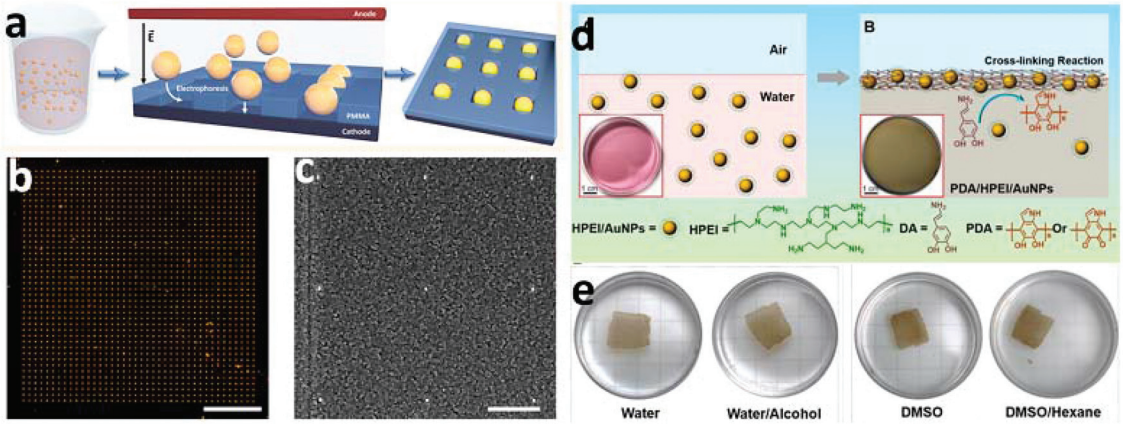

Fig. 8 Typical examples for constructing 2D MFGS by other approaches except interfacial assembly. (a–c) Electrophoretic deposition:[132] (a) schematic of the preparation of 2D MFGS *via* electrophoretic deposition of Au NPs on a predefined patterned substrate; dark-field image (b) and SEM images (c) of Au NR arrays on the patterned substrate. Scale bar: dark-field images, 40 μm; SEM, 2 μm. (d and e) *In situ* reduction to construct 2D MFGS:[135] (d) schematic of *in situ* reduction of $HAuCl_4$ into HPEI-functionalized AuNPs and formation of 2D MFGS cross-linked with PDA; and (e) transferring the prepared cross-linked 2D MFGS on various liquid surfaces.

changes, such as temperature, humidity, and pressure. (3) Mechanical strength. Pure 2D MFGS are easily breakable. (4) Controllable LSPR. It is difficult to obtain 2D MFGS with controllable gaps and components. (5) Electrical conductivity. It is highly important and difficult to tune the conductivity of a 2D monolayer, due to the inevitable space between neighbouring NPs in the monolayer. Therefore, it is vital to overcome these obstacles and broaden the applications of 2D MFGS. Surface functionalization of 2D MFGS endows them with desired properties or new distinctive performances. In this section, the functionalization of 2D MFGS is systematically summarized according to the properties of 2D MFGS.

4.1 Enhancing the conductivity of 2D MFGS

Noble metal nanoparticles (such as gold, silver, and platinum) exhibit good electronic transmission performance, which enables their wide applications in biosensors and electronic devices.[136,137] However, the conductivity of Au NP monolayers is not satisfactory for applications due to the discontinuous electronic transmission resulting from large and uncontrollable void space between neighbouring NPs. Therefore, much effort has been devoted to achieve prominent conductivity by the functionalization of 2D MFGS with mercaptoalkanes and other conductive materials such as graphene oxide (GO) and conductive polymers.

Functionalizing 2D MFGS with mercaptoalkanes is an efficient approach to enhance the conductivity of 2D MFGS, in which the charge transport between Au NPs can be conducted through mercaptoalkanes.[138] It is noteworthy that $-CH_2-$ groups are considered as insulators and the charge transmission *via* molecules is often governed by the nature of molecules. The Fermi level of the metal (such as gold) is located in the HOMO–LUMO gap of the molecule and the electrons can tunnel along the molecule through the side orbitals.[139] The electronic conduction mechanism of mercaptoalkane functionalized 2D MFGS is a thermally activated conduction pathway and the conductivity depends on the core radius (r), interparticle distance (d), permittivity constant (ε_0), and dielectric constant of the interparticle medium (ε).[140,141] The activation energy (E_a) can be calculated according to Murray's[17] Arrhenius-type activated tunnelling model (eqn (2)) as follows:

$$E_a = 0.5e^2 \frac{r^{-1} - (r+d)^{-1}}{4\pi\varepsilon\varepsilon_0} \quad (2)$$

This suggests that the activation energy increases with the interparticle distance and decreases with the particle size. Therefore, the chain length of the mercaptoalkanes is particularly important for the conductivity of 2D MFGS. Zhong's group has made outstanding contributions in investigating the conductivity of Au NP monolayers by coating Au NPs with mercaptoalkanes.[142,143] They found that the conductivity of alkyl dithiol coated Au NP monolayers gradually decreased with an increase in the $-CH_2-$ unit (n) in the alkyl dithiols.[140] Similar results have been reported by Yang and co-workers (Fig. 9a and b), who fabricated alkylamine coated Au NP monolayers by ethanol induced water–hexane (with alkylamine) interface assembly.[144] The combination of Au NPs with a polymer is another efficient approach to enhance the conductivity of 2D MFGS.[145–147] Generally, polymers are used to achieve high conductivity of 2D MFGS, and they can be divided into two families: (1) elastomeric polymers (such as polyurethane (PU) and polydimethylsiloxane (PDMS));[148–150] and (2) conductive polymers or polyelectrolytes (polyaniline for example).[151,152] Regulating the particle gap by applying external force is impossible for adjusting the conductivity because of the lack of a self-supporting property and incapable bending of 2D MFGS. The elastomeric polymer functionalization can effectively solve the problem and endows the 2D MFGS with controllable supporting and bending properties. For instance, Lee's group[153] constructed conductive 2D MFGS

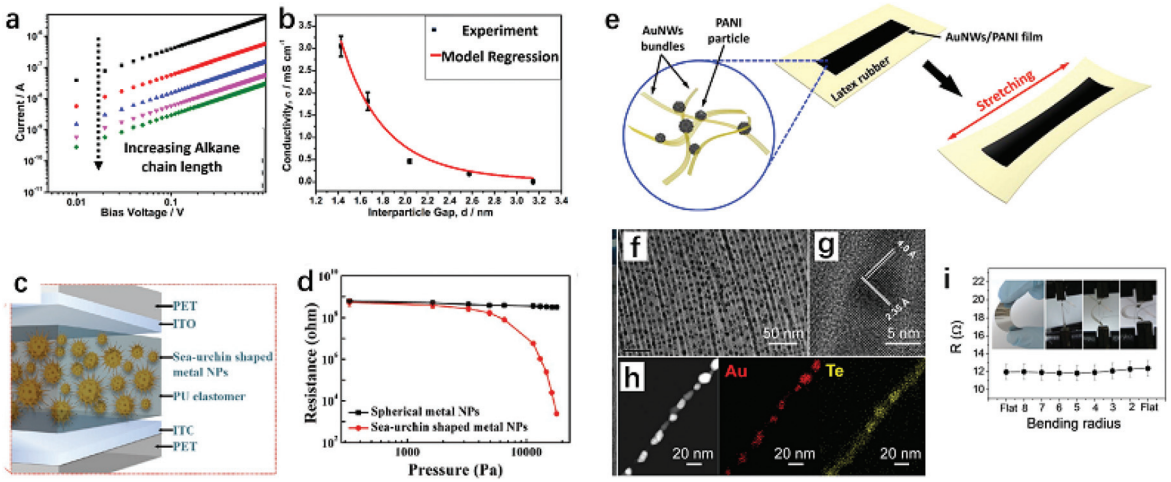

Fig. 9 Typical examples of functionalization of Au NPs to enhance the conductivity of 2D MFGS. (a and b) Alkane chain modification improves the conduction of Au NPs:[173] the influence of alkyl chain lengths (a) and interparticle gaps (b) on the conductivity of the 2D Au NP monolayers. (c and d) Polymer modified 2D Au NP films to enhance the conductivity:[153] (c) schematic illustration of construction of piezoelectric materials based on Au NPs and an elastomer (PU); piezoresistive characteristics (d) of the composited piezoelectric materials; (e) another example of PANI modified 2D Au NP films to enhance the conductivity.[151] (f–i) Composite 2D films for enhancing conductivity:[174] (f–h) TEM, HRTEM and STEM-EDS elemental mapping images of the ordered Au–Te hetero-monolayer with different magnifications; and (i) the relationship between the bending radius and the conductivity of the 2D Au–Te-PET films.

consisting of an insulating PU elastomer and sea-urchin shaped gold nanoparticles (SSNPs) by spin-coating a mixture solution of a PU monomer and SSNPs on an indium tin oxide substrate (Fig. 9c and d). Although the insulating PU elastomer and separated SSNPs were incapable of forming a pathway for electron transport, the quantum tunnelling effect[154] occurred between the tip parts of SSNPs and the electrons leap or tunnel from the SSNP to the neighbouring one. As a result, the conductivity of the 2D SSNP film was significantly improved and it is utilized in pressure sensing. In addition, the conductivity of 2D MFGS is related to the morphologies of Au NPs. Au nanowires (Au NWs) often show relatively high conductivity due to their ultrathin nature.[155] However, their conductivity remains low compared to other conductive materials. Cheng's group[151] functionalized Au NWs with conductive PANI microparticles to construct composite conductive films, which enhanced the conductivity up to 10 times compared with that of bare Au NW films (Fig. 9e). Other polyelectrolytes such as poly(allylamine hydrochloride) (PAH) have also been used to strengthen the conductivity of 2D MFGS. Besides, the conductivity was sensitive to the relative humidity. The swelling of the polyelectrolyte chains between adjacent particles resulted in larger gaps and lower tunnelling probabilities.[152] Finally, other conductive materials (such as graphene) were used to enhance the conductivity of 2D MFGS.[156,157] Yu's group introduced tellurium (Te), which is a p-type helical semiconductor with a narrow bandgap energy of 0.35 eV, to construct 2D Au–Te NW composite 2D monolayers (Fig. 8f–i). The electrical conductivity is as high as 10 000 S cm^{-1} and the application can be extended to light-emitting diode (LED) arrays by transferring the composite 2D monolayer on a flexible PET substrate.[158]

4.2 Enhancing the optical properties of 2D MFGS

The unique optical properties of Au NPs have been well-known as early as in ancient Roman ages (the famous "Lycurgus Cup").[137] Various optical applications have been advanced based upon the LSPR property of Au NPs.[159–162] Compared with individual Au NPs, 2D MFGS often exhibit more fascinating electromagnetic properties, which facilitates their applications in sensing, detection, electrochromic displays and photovoltaic devices.[163–165] Similar to the conductivity, the optical properties of 2D MFGS are strongly dependent on the size, interparticle distance and dielectric constant of Au NPs.[166–168] For instance, the SERS detection mechanism is closely related to the local confinement of the electromagnetic field that is especially strong within plasmonic hot spots in close-packed Au NPs.[10,169] Therefore, regulating these parameters can effectively control and optimize the optical performance of 2D MFGS. The regulation of particle space during film forming is an efficient approach to tune the optical performances and applications.[169–172]

Kornyshev's group prepared dense MFGS with controllable particle gaps with the assistance of an electrochemical liquid–liquid cell.[175] As shown in Fig. 10a, the dense "golden mirror" was prepared *via* forming a violent "potential energy well" induced by screening the electrolyte.[176] With increasing time, the space between neighbouring Au NPs changed, resulting in the variation in the reflectivity of light. The absorption spectrum of the Au NP film can also be adjusted by controlling the distance between adjacent Au NPs. Hanske and co-workers[177] achieved controllable absorption of light that nearly covers the entire range of the solar spectrum by modulating the gap

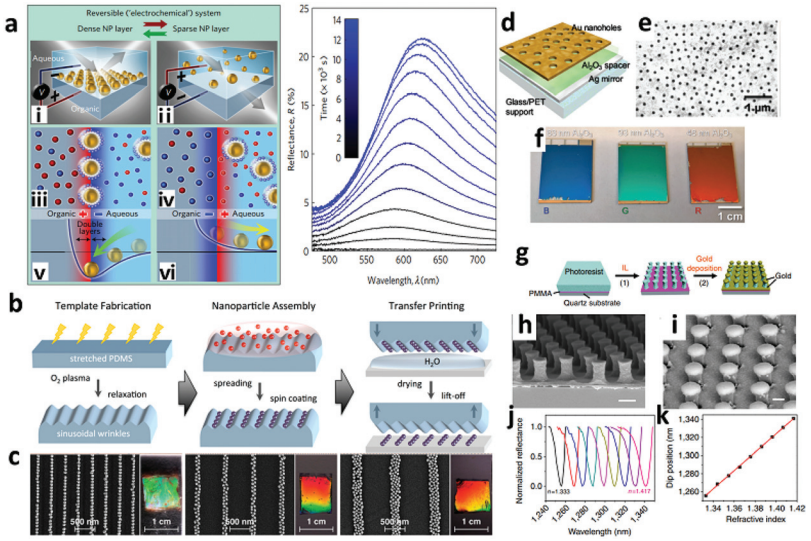

Fig. 10 Nanoplasmonic liquid mirror strategies for constructing 2D Au NP monolayers with wide reflective properties:[175] (a) schematic illustration of the electrochemical liquid–liquid cell for forming 2D MFGS and the electrochemical liquid–liquid cell with an optical probe and the broad reflective ranges achieved by adjusting the density of 2D Au NP monolayers; (b) modulating the gap between adjacent Au NPs.[177] (c) Optical characterization and TEM of nanoparticle chain assemblies of the 2D MFGS with various quantities of particle chains; (d–f) plasmonic metasurfaces for widening the reflective chromogenic range of Au nanohole based films:[44] (d) schematic of the metasurface; (e) electron microscopy image of the Au nanoholes; (f) a photograph of the metasurfaces with various colors under ambient light; (g–k) construction of Au mushroom arrays on a PMMA substrate to achieve an ultra-sensitive optical response:[183] (g) schematic illustration of the preparation procedure; (h and i) SEM images of 2D Au mushroom arrays on the PMMA substrate; and (k) optical sensitivity characterization of the 2D Au mushroom arrays.

between adjacent Au NPs (Fig. 10b and c). In addition, fixing Au NPs to the pre-set position can help achieve controllable gaps in Au NP films.[178,179] Lee and co-workers[180] utilized PS-*b*-P4VP arrays as templates to induce the growth and assembly of Au NPs. With increasing growing time, the gap between neighbouring Au NPs decreased and the optical properties of 2D MFGS changed accordingly. Moreover, the morphologies of the Au NPs also show distinct significance in the optical properties of 2D MFGS,[181] as reported by Nguyen and co-workers.[182] Many investigations have been conducted to explore the optical properties of isolated Au NPs on metal films, in which an intense coupling effect was generated between the NPs and the metal film.[184–187] Nevertheless, Au NP arrays on metal films are more attractive than individual Au NPs.[188] The enhanced optical properties originated from the additional momentum, which can couple the incident light with surface plasmon polaritons on the metal film.[189–191] Therefore, tuning the dielectric environment around the Au NPs, and the space between the Au NPs and metal films would help achieve controllable optical performance of 2D MFGS. Xiong *et al.*[44] achieved naked color regulation (red, green, and blue) *via* adjusting the thickness of an alumina spacer between Au nanoholes and a Ag mirror (Fig. 10d–f). It is well-known that Au NPs in 2D films often show a red-shift and a broad LSPR peak compared with individual Au NPs in solution due to the overlap of the electron wave function between adjacent nanoparticles.[144] But it is unfavourable for the use of 2D MFGS in LSPR sensor application, as the broad LSPR is not clearly sensitive and changes as the local refractive index changes.[192,193] Shen and co-workers[183] constructed submicrometer Au mushroom arrays on a poly(methyl methacrylate) (PMMA) substrate that gained apparent refractive index sensitivity due to the coupling of LSPRs with Wood's anomaly, which diffracted the incident light into a propagating wave (Fig. 10g–k).

4.3 Functionalization for other purposes

As mentioned above, there are many disadvantages such as poor stability and low mechanical strength of 2D Au NP films. To address these issues, introducing other available structures such as a core–shell structure and polymer coating of particles is the most efficient means. For instance, as a stable and accessible material, silica (SiO_2) has been a useful component to enhance the stability of Au NPs.[194–196] In addition, some elastomer polymers were utilized to achieve high mechanical strength for sensing devices.[145,165,197] Particularly, DNA molecules are powerful ligands to construct free-standing 2D MFGS. Luo's group firstly achieved 2D free-standing Au NP superlattices *via* DNA base pairing in a drying-mediated self-assembly process (Fig. 11a–c).[198] Additionally, the inter-particle spacing can be adjusted by tailoring the DNA length. Estephan and co-workers[199] reported the construction of responsive free-standing films *via* self-assembling of DNA modified Au NPs with unique sharp melting transition properties, as shown in Fig. 11d and e. Generally, DNA molecule interaction has been an effective approach to obtain free-standing 2D MFGS with high mechanical strength. More importantly, the controllable

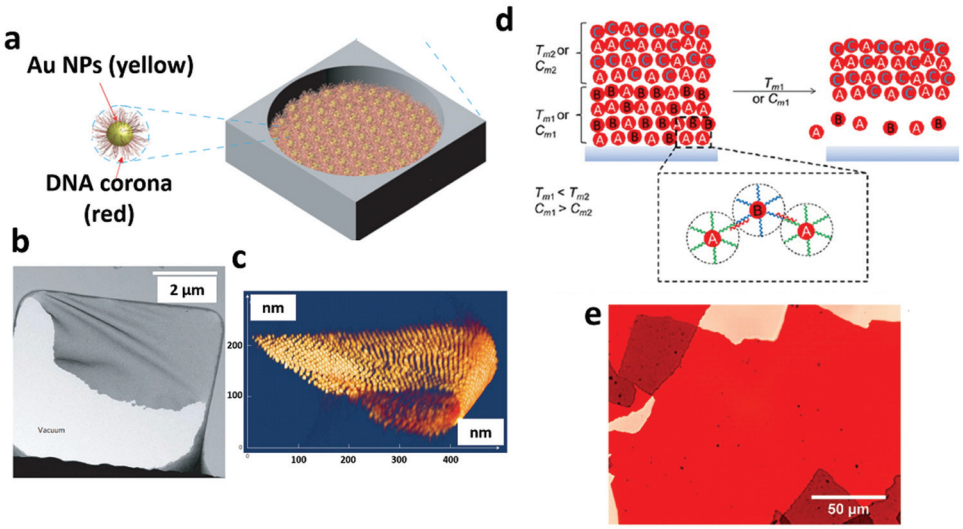

Fig. 11 Typical examples of functionalization of Au NPs with DNA to enhance the mechanical strength of 2D MFGS. (a) Schematic diagram of construction of 2D MFGS *via* the interaction of DNA coated Au NPs;[198] (b) TEM image of a DNA coated superlattice sheet partially attached to a 7 × 7 μm hole in the carbon substrate; (c) 3D STEM tomography reconstruction of a folded sheet. (d) Schematic diagram of the self-assembly of DNA modified Au NPs with controllable melting transition properties;[199] optical microscopy images (e) of Au NP assemblies.

length and designable features of DNA molecules enable more applicability of the assemblies.

5. The applications of 2D MFGS

The plasmon resonance performance of 2D MFGS is greatly amplified relative to that of the independent nanoparticles, which is derived from a close conjunction of the localized plasmon resonance between adjacent gold nanoparticles. Therefore, combined with their large specific surface area and good conductivity, 2D MFGS are widely explored in various applications, especially fields using plasmon-enhanced optical signals such as fluorescence enhancement and SERS. When it comes to the optical fields, it is still challenging to interact light with 2D materials, which results in reduced light absorption and emission.[200] However, 2D MFGS can efficiently activate the plasmon-enhanced effects. Nowadays, 2D MFGS are being widely applied in the optical fields involving fluorescence enhancement,[201–205] SERS enhancement[10,84,206,207] and plasmon based optical devices.[208–211]

5.1 Enhanced fluorescence for detection in biosensors

The mechanism of metal enhanced fluorescence (MEF), especially Au NP enhanced fluorescence (AEF), has been investigated for many years. The key issues behind the enhancement of fluorescence by Au NPs and finding ways to maximize the fluorescence enhancement *via* tailoring the size and morphologies of Au NPs and the distance between Au NPs and fluorescent molecules are discussed.[212,213]

The fluorescence emission process is composed of absorption and emission of light, which are quantitatively determined from the excitation efficiency and fluorescence quantum yield, respectively (Fig. 12). The following two parameters determine the fluorescence emission intensity.[213,214] (1) The excitation enhancement occurs by coupling a fluorophore with the nearby Au NPs. In other words, strong local electric fields arising from the excitation of the LSPR of Au NPs can highly enhance fluorescence. (2) The increase of the radiative decay rate or the energy transfer originates from the surface-plasmon resonance-coupled excited state of the fluorophore.[215,216] Generally, the fluorescence quantum yield (Q_0) is determined from the radiative decay rate (Γ) and non-radiative decay rate (k_{nr}). The computational expression is as follows:

$$Q_0 = \frac{\Gamma}{\Gamma + k_{nr}} \quad (3)$$

The effect of the metal should be considered in the presence of metallic structures; so the computational expression is modified as:[217,218]

$$Q = \frac{\Gamma + \Gamma_m}{\Gamma + \Gamma_m + k_{nr} + k_m} \quad (4)$$

The metal was considered as an optical antenna that converted the propagating radiation to near field energy to further enhance the fluorescence quantum yield.[219]

There are still many disadvantages that limit the application of Au NP based AEF: (1) the disordered arrangement of hot spots. As mentioned above, the appearance of the strong local electric fields is of great importance for AEF. The local electric fields were usually produced around the fields of hot spots.[220] As noble metal nanoparticles usually dispersed homogeneously in water, they often present a disorderly arrangement. Hence, the natural disorderly arrangement of hot spots limits the enhancement of the fluorescence intensity

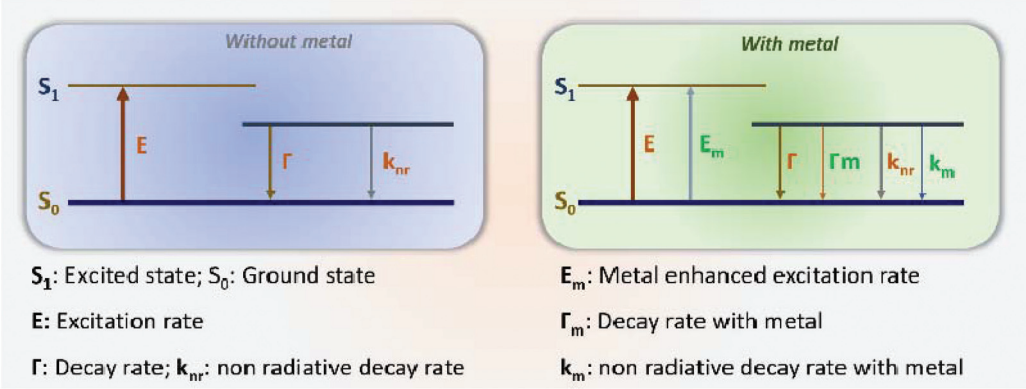

Fig. 12 The simplified Jablonski energy level diagram.

maximum. (2) The uncontrollable distance between the fluorophore and Au NPs. The introduction of a filler is usually used for AEF. However, it is challenging to design handy AEF systems due to the existence of particle space.[221,222] More importantly, coating Au NPs with a shell (polymer, silica and so on) often causes the shift of the LSPR wavelength,[223,224] which makes it difficult to match the excitation wavelength of the proposed fluorophores. (3) The stability of the fluorescence intensity of AEF. The fluorophores often bind to the surface of the coating shell by physical methods, which makes it uncontrollable.[225]

2D MFGS possess great potential superiority in addressing the issues in MEF. (1) The controllable arrangement of hot spots. Particularly, hot spots formed by anisotropic gold nanoparticles are often concentrated in some specific areas.[226–228] (2) Easily controllable space. As mentioned above, for nanoparticles in solution, the coating shell was used to control the space between the nanoparticle and the fluorophores, which makes it more complicated and less controllable.[229] However, for the 2D nanoparticle arrays, there is no need to induce an uncontrollable shell to adjust the gap between the hot spots and the fluorophores. Instead, some telescopic molecules (such as DNA, stimulus-responsive polymer) can act as spacers, and precisely regulate the gap to an appreciable value. (3) Coupling enhanced fluorescence. The gold nanoparticles in 2D MFGS often arrange densely. More importantly, the distance between the gold nanoparticles is immobilized and unified. Thus, the coupling between the gold nanoparticles would produce a strong electric field,[207] and enhance the fluorescence intensity to a great extent.

There are a great deal of advantages of 2D MFGS based AEF systems. As shown in Fig. 13a and b, Shi and co-workers have investigated the fluorescence enhancement by depositing QDs on top of a Au nanocube self-assembly.[43] The droplet forming method was used to fabricate uniform Au nanocube monolayers at a large scale. Due to the coupling of Au nanocubes with QDs, the enhancement factor was up to 3.5 times. Other than isotropic gold nanoparticles, some anisotropic gold nanoparticles are also applied for constructing monolayer based AEF systems. Tang and co-workers[231] have studied the AEF effect based on the Au NRs arrays (Fig. 13c and d). Au NR assemblies with a controllable arrangement were prepared for constructing a hot spot-controllable AEF system. In addition, the fluorescence enhancement of the Au NR array-based AEF system was dependent on the DNA length. The appropriate gap (less than 16 nm) would result in high fluorescence enhancement. It is noteworthy that only Au NRs with a highly controllable arrangement can realize maximum fluorescence enhancement compared with random ones. This indicates that the overlap of the LSPR wavelength with the excitation wavelength of the fluorophores is very important for enhancing fluorescence. Additionally, it is more important to achieve AEF at near-infrared (NIR) and second NIR (NIR-II) biological windows for AEF based biological applications.[108] Xie's group[201] achieved AEF at these biological windows by constructing Au nanostar arrays. Fluorescence enhancement of more than 320-fold in the NIR region and 50-fold in the NIR-II region was achieved with this AEF-NIR system (Fig. 13e–g). Moreover, the tunable plasmon response in the NIR-II region for Au NP arrays can be also achieved by nanoscale control of the structure of Au NPs (Fig. 13h). Xie's group[230] modulated the conduction of colloidal lithography and obtained Au NP arrays with various structures which were adapted to QDs for the greatest fluorescence enhancement.

5.2 SERS enhancement

The discovery of surface-enhanced Raman scattering (SERS) was made nearly 30 years ago, which opened a new avenue for Raman spectroscopy.[231,232] The dramatic enhancement of the vibrational spectra from the analyte adsorbed on a rough (at the nanoscale) metal surface has been intensively investigated to understand the underlying physical phenomenon. The mechanism of SERS enhancement has been debated in academic circles for many years, and generally there are two main types of enhancement mechanisms: electromagnetic enhancement and chemical enhancement. (1) Electromagnetic enhancement is caused by the collective vibration of conduction electrons in metal nanoparticles. When light hits the

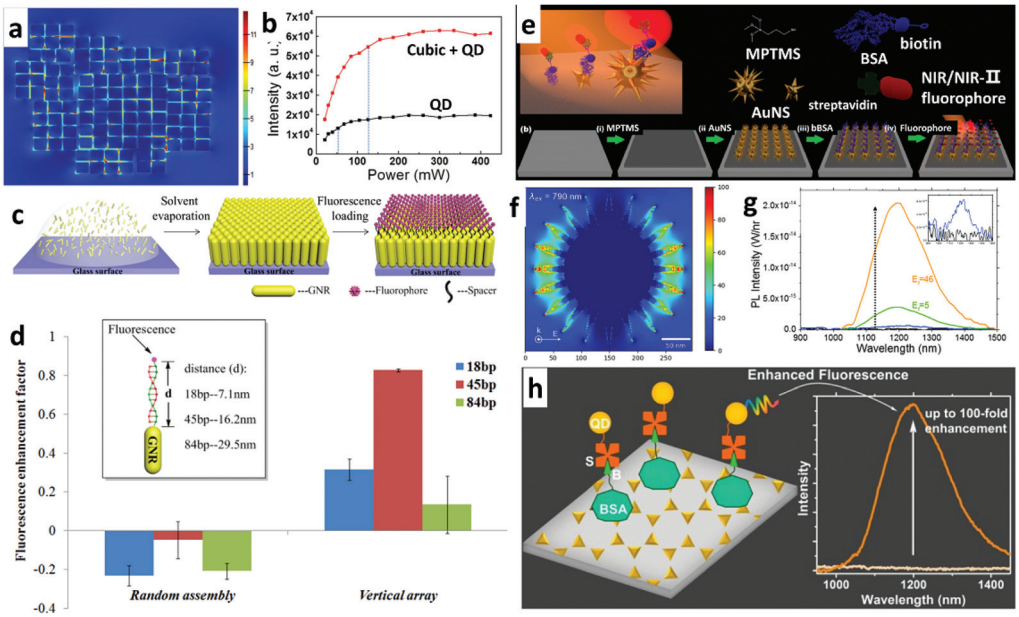

Fig. 13 (a and b) Enhanced photoluminescence based on Au NC assemblies:[43] SEM images (a) and field distribution (b) of the Au NC self-assembled structure; (c and d) amplification of the fluorescence signal by coupling fluorescent molecules with ordered Au NR arrays:[215] (c) schematic of the preparation of a Au NR array enhanced fluorescent system; (d) the comparison of fluorescence enhancement between random Au NR assemblies and Au NR arrays; (e–g) Au nanostar ordered substrates for enhancing fluorescence:[201] (e) schematic illustration of the construction the near-infrared fluorescence detecting platforms based on Au nanostar arrays; (f) the electromagnetic field enhancement of Au nanostars calculated by finite-difference time-domain (FDTD) modeling; (g) the fluorescence enhancement of Au NP arrays for different Ag_2S QDs by oxidizing the polystyrene template at different times; (h) adjusting the structure of Au NPs for enhancing fluorescence:[230] schematic illustration of fluorescence enhancement on Au NP arrays.

surface of the precious metal nanoparticles, free electrons in the noble metal surface are quickly induced and vibrate, creating a local electromagnetic field. The excitation of the surface plasma will result in the enhancement of the local field of the adsorbed molecules on the nanoparticle surface.[232,233] Although this enhancement has its limitations, the overall effect often shows an enhancement of several orders of magnitude.[234] (2) Chemical enhancement is another independent mechanism, which mainly enhances the Raman scattering of molecules adsorbed on metal surfaces.[235] Chemical enhancement can be divided into three mechanisms. (a) The adsorption molecule chemical bond to the metallic substrates, which results in non-resonant enhancement. (b) The adsorption of the molecule and the surface adsorption of the atoms form a complex to contribute towards resonance enhancement. (c) Class resonance enhancement. Photo-induced charge transfer induced by light excitation. It is noteworthy that the electromagnetic field enhancement near metallic nanostructures dominated SERS applications. The surface plasmon coupling at the junctions or gaps between these structures forms hot spots with enormous enhancement for high-sensitivity SERS detection. The function of the nano-substrate is important for the electromagnetic enhancement while the chemical enhancement was achieved by adjusting the electron density of the pending molecule. The current obstacle is the lack of highly sensitive, stable, and widely prepared SERS substrates.[236,237] For the optimal SERS substrate, the following conditions must be available: high sensitivity, good uniformity, environment friendly nature, exceptional stability and repeatability, and cost-effectiveness.

Given that noble nanoparticle substrates contribute substantially towards the enhancement of SERS signals, most works were conducted to achieve SERS detection based on noble nanoparticle substrates. Depositing NPs on various substrates to construct SERS substrates is the most frequently used strategy for enhancing SERS detection signals. The regulation and optimization have been concentrated on adjusting the morphology and species of noble nanoparticles. Yang's group[238] investigated the influence of the morphology of nanoparticles on SERS detection. However, the SERS signal of the silver nanoparticles with various shapes displayed great differences after detecting the single-particle scattering spectra. In addition, Xu and co-workers demonstrated that the noble nanoparticles with sharp structures often exhibited high SERS signals.[239] Recently, the heterogeneous structures of noble nanoparticles have become increasingly popular in SERS detection. Qin's group investigated the influence of heterogeneous nucleation on SERS enhancement by depositing the second metal on Ag nanocubes.[240]

Our group has prepared "SERS tape" by combining the adhesive tape with 2D MFGS (Fig. 14a and b).[76] The transparency, adhesiveness, and flexibility of the tape would enable close contact with the complex surface and high sensitivity to the targets.[90] Nowadays, some biological creatures are being

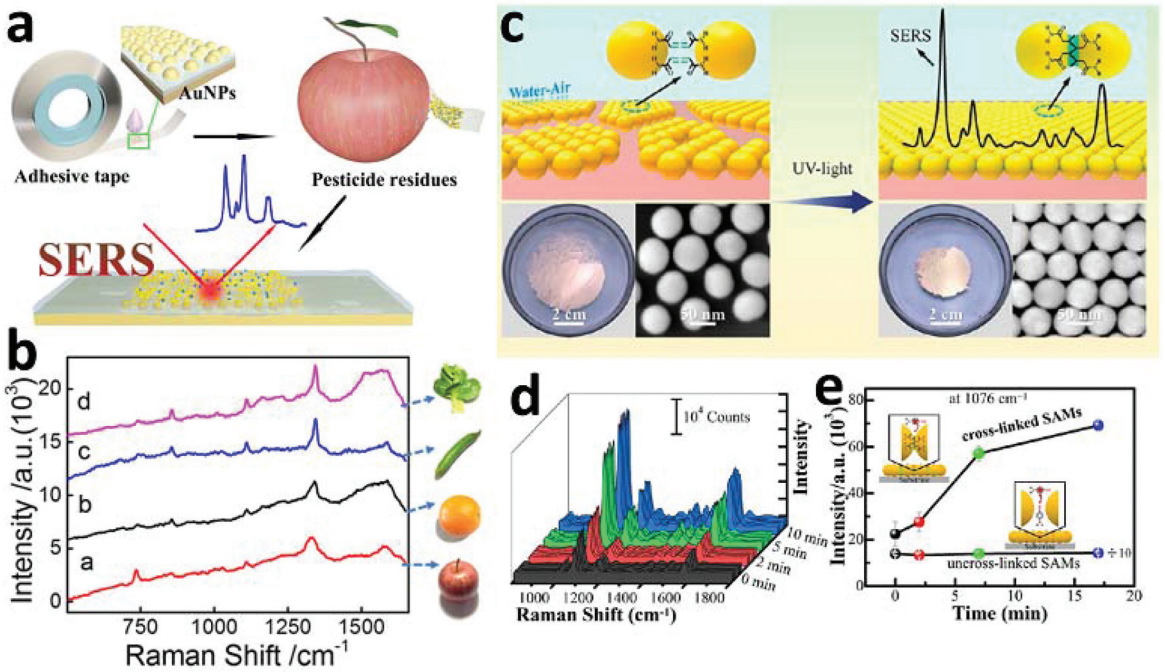

Fig. 14 SERS tape for the analysis of practical samples: (a) schematic illustration of the preparation of Au NP based 2D SERS tape for SERS analysis; (b) Raman spectra of practical samples collected from Au NP modified adhesive tapes;[76] (c) cross-linked 2D MFGS monolayers for SERS detection:[3] (d and e) SERS detection properties of the cross-linked monolayer films: cross-linked and un-cross-linked monolayers for SERS detection of 4-ATP (10^{-4} M); and (k) stability assessment of the cross-linked monolayers at different irradiation times.

used for scientific research studies. As a talented wall walker, geckoes have a large contact area produced by the high density of nanoscale tentacles on their toe-pads. This was used to construct a SERS substrate with a gecko-like multiscale structure.[77] It is well-known that 2D MFGS with tuneable gaps offered accurately controllable hot spot distribution. Our group achieved highly sensitive SERS detection with excellent stability by utilizing chemically cross-linked 2D MFGS (Fig. 14c–e).[3] The tuneable nanogap and uniformity of the 2D MFGS made them a smart candidate in the SERS field of detection.

Although pure Au NPs have significantly enhanced the detection sensitivity (10^8)[89], they often tend to aggregate which makes it difficult to acquire a uniform 2D SERS substrate, resulting in low reproducibility of the SERS signals.[88] In recent years, multicomponent nanomaterials, especially core–shell nanomaterials, have attracted great attention in SERS detection.[86,241] The core–shell NPs exhibited numerous advantages compared with pure noble metal NPs: (1) the combination of different materials which expends the application of pure Au NPs; (2) the tunability of the composite materials: the shape, size and thickness of the shell;[242] and (3) stability and reproducibility: the existence of shell materials can extremely enhance the stability of the pure noble metal NPs. Moreover, the shell materials can be beneficial for the assembly of NPs, which can improve the reproducibility of SERS detecting signals.[85,88] In the current study, there are several major types of core–shell materials that have been widely applied in SERS detection: (a) Ag shell coated Au nanoparticles. As we know, Ag displays a much broader SERS enhancement region ranging from 400 nm to the near-IR region compared with Au NPs in SERS detection.[96,243,244] As shown in Fig. 15a–c, Gao and coworkers synthesized porous Au–Ag alloy nanoparticles to concentrate the "hot spot" and therefore enhanced the sensitivity to analytes.[83] Additionally, the Au–Ag alloy nanoparticles were encased in ultrathin hollow silica shells to improve the stability. The composite system showed excellent SERS activity with an enhancement factor up to ~1.3×10^7 under off-resonant conditions. (b) Inorganic oxide material coated Au NPs. Nowadays, many inorganic oxide materials (SiO_2 and MnO_2) with good stability and accessibility are being applied in SERS detection by combining them with noble nanoparticles. Tian's group has devoted considerable effort in this field for many years, and results are shown in Fig. 15d.[62,245] Ultrathin MnO_2 or SiO_2 shell coated Au nanoparticles were prepared to construct the so-called "smart dust" for SERS detection with high sensitivity and reproducibility. (c) The core–shell nanomaterials with intelligent response to analytes. In recent years, some smart SERS substrates with special properties have been investigated. As shown in Fig. 15e, Fan's group invented a smart SERS substrate with self-cleaning function by coating Au NPs on TiO_2 2D arrays.[92] The self-cleaning function of the proposed system originated from photocatalytic degradation of the target molecules by TiO_2. As we know, the gaseous molecules are difficult to be distinguished due to their low absorptivity on a solid substrate and weak Raman scattering. Wang's group[246] constructed a SERS capturing channel for volatile

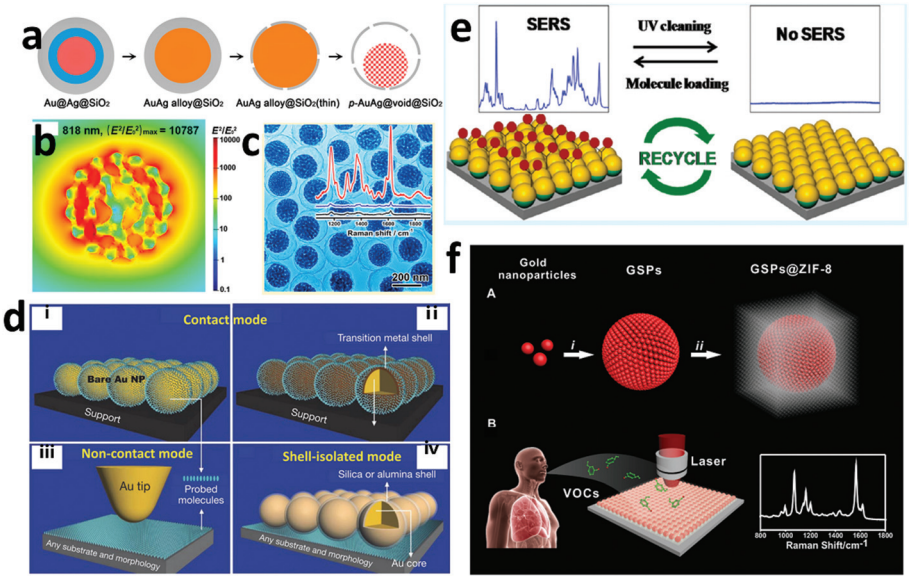

Fig. 15 (a) Synthesis of p-AuAg@void@SiO_2 yolk/shell NPs by a dealloying method; (b) simulated near-field electromagnetic field distribution of the p-AuAg@void@SiO_2 yolk/shell NPs by an incident plane wave of 818 nm; (c) a schematic representation of the p-AuAg@void@SiO_2 yolk/shell NPs and the SERS enhancement of the proposed composite system;[83] (d) three different working principles of the traditional SERS enhancing model:[253] the contact mode of Au NPs (i–ii) and Au core–transition metal shell NPs (iii), non-contact mode of tip-enhanced Raman spectroscopy (iv) and shell-isolated mode of shell-isolated Au NPs; (e) the ordered arrays of the Au nanoshell on TiO_2 NPs to achieve ultrasensitive and recyclable SERS detection;[92] (f) construction of Au NPs-ZIF-8 composited arrays for ultrasensitive VOC detection:[246] diagrammatic sketch of the preparation of Au NP-ZIF-8 composites and VOC detection *via* SERS spectroscopy.

organic compounds (VOCs) by coating Au NPs with a ZIF-8 layer (Fig. 15f). Gaseous aldehydes (tumor-specific tissue composition and metabolism, such as formaldehyde) were immobilized on the Au NP SERS substrate through the ZIF-8 channel by a Schiff base reaction with 4-aminothiophenol (4-MBA). Besides, there are some other approaches to optimize the SERS detection performances. In a word, exploring a SERS substrate with high stability, excellent sensitivity and outstanding selectivity is always desired for SERS detection.

5.3 2D MFGS based optical devices

Nowadays, the applications of nanoparticles in constructing devices are a hot field of current research.[167,247–249] 2D MFGS exhibit unique superiority in plasmonic switching devices due to the highly sensitive response of LSPR to the external environment.[250–252] Herein, 2D MFGS based optical devices would be classified into plasmonic switched dynamic discoloration and information storage.

5.3.1 Plasmonic switched dynamic discoloration. Plasmonic switching refers to the on–off response performance of Au NPs to an external stimulus, and the response is usually presented in the form of a spectrum or color variety.[167,254,255] Although the shape of particles, surface molecular distribution[256] and crystal plane have great influence on the plasmonic response,[257] it is often achieved *via* modulating the distance between the Au NPs and the dielectric environment around the particles.[254,258] The plasmonic switched dynamic changes for individual Au NPs in solution are often determined with stimuli-responsive molecules.[259] For instance, modifying Au NPs with an amphiphilic polymer to adjust the assembly and disassembly under different solvent environments is an effective approach to achieve switched dynamic spectral changes.[260] However, the harsh reaction conditions and limited amounts enormously restrict the application of plasmonic switched dynamic discoloration. Thus, a growing number of research studies constructed switched dynamic discoloration systems based on 2D MFGS. Reflective displays are an important research trend in the field of plasmonic dynamically reconfigurable discoloration, due to the wider viewing angles and comfortable visual experience.[45] Particularly, the Kretschmann configuration[261,262] achieved a switchable plasma switch response driven by the changing external environment, in which the stimulus response layer was anchored between the Au NPs and metal substrates. Kim's group[263] combined a Au substrate with temperature-sensitive poly(*N*-isopropylacrylamide) (PNIPAM) linker layer modified Au NPs to present sensitive reflection spectrum switching (Fig. 16a and b). In addition, some other responsive polymers (such as pH sensitive poly(2-vinylpyridine) (P2VP) polymer brushes) were also utilized to achieve plasmonic switched spectral changes (Fig. 16c).[264,265]

Currently, modern nanotechnology and engineering in turn raise a demand for different plasmonic reversible switching techniques. As one unique "pigment", 2D plasmonic materials provide high contrast, high resolution, and everlasting colors, which has become the focus of research.[266,267] However, it is always difficult for 2D plasmonic materials to achieve bright and rich colors.[45] Much effort has been devoted to improve the

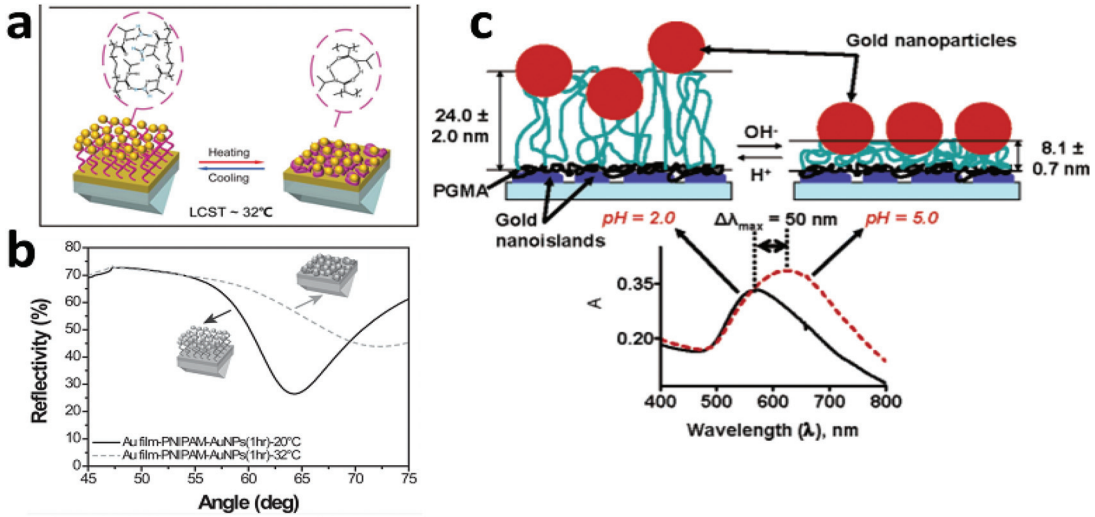

Fig. 16 The Au film-pNIPAM-Au NP assemblies for reversible plasmonic switches:[263] (a) schematic representation of the reversible plasmonic switches at different temperatures of the Au film-pNIPAM-Au NP assemblies; (b) reflective curves of Au film-PNIPAM-AuNPs with different areal densities of AuNPs acquired by immersing the Au film-PNIPAM into Au NP solution for different times; and (c) coating Au NPs with a pH sensitive polymer (poly(2-vinylpyridine), P2VP) to achieve reversible plasmonic switches.[265]

colorfulness of the pigment (Fig. 17a and b). The conductive polymer (polypyrrole) possesses distinct switched light capture capabilities under oxidized and reduced states, which can be utilized to achieve switched and rich color changes.[44] Nevertheless, the relatively complicated manipulation and introduction of an external field makes it inconvenient for use. Our group[268] achieved dual-responsive plasmonic switches by modifying Au NPs with a dendronized copolymer, which is pH and temperature sensitive (Fig. 17c–f). The switched dynamic discoloration resulted from the obvious spacing variation between Au NPs in the monolayer, which was derived by the responsive dendronized copolymer. Besides, perfect dynamic discoloration often requires color changes in the full visible range and is multi-color switchable. As we all know, different kinds of noble metals have diverse absorption bands for light. The combination of various noble metals is an efficient approach to achieve the multi-color switchable property. Chu and co-workers[269] deposited Ag layers with tuneable shell thicknesses on Au nanodome arrays to achieve color changes in the full visible region (Fig. 17g–i). In addition, mechanical chameleons were constructed for monitoring active camouflage with the rapid multi-color switchable properties.

5.3.2 Information storage. The twenty-first century is the big data era. Ultra-low energy consumption to generate, transmit and store information is currently in demand.[270] Optical information storage has attracted increasing attention in various fields ranging from economics to education,[271] due to the high capacity data storage and long-time security.[272] 2D MFGS have been widely applied in data storage, due to the apparent colour change resulting from the particle distance and morphology variation. Kornyshev's group achieved dynamic anti-counterfeiting information display switching by utilizing 2D MFGS with controllable distances between adjacent Au NPs (Fig. 18a and b).[175]

Although progress is being achieved at a miraculous pace, there are still two tough issues hindering the development of optical information storage: (1) the diffraction-limit barriers restricting system resolution; and (2) high-capacity optical data storage. It is well-known that Au NPs often present shape-dependent LSPR (Fig. 18c). Au NPs with various morphologies often show a distinct capturing ability for different light sources. Reshaping of Au NPs under the resonant excitation of a femtosecond (fs) laser is an effective method to achieve high optical information storage.[273] The superior frequency and polarization dependence of Au NPs (especially anisotropic Au NPs) make it possible for 2D MFGS to break the diffraction-limit. Our group[274] investigated the polarization dependent optical properties of Au NRs by tuning macroscopic-oriented Au NRs in the PVA-Au NR composite films (Fig. 18d–f). In addition, single or a few nanoparticles in the Au NP arrays (2D MFGS) as information writing units enormously increase the storage capacity.[275]

Gu's group have devoted much effort towards plasmonic NP based optical information storage for many years and have made outstanding contribution towards promoting the development of electronic information engineering.[273,276] For example, they proposed the "5D optical recording" firstly based on the reshaping of disorderly distributed Au NRs (Fig. 18g–h).[277] By utilizing the plasmon information units of Au NRs in PVA-Au NR composite films, they acquired a storage capacity of 1.6 TB for a disc the size of a DVD and broke the diffraction-limit. Besides the high capacity, multicolor information storage is another important issue that needs to be addressed in Au NP based information storage.[45] Recently, Roberts and co-workers[278] proposed an innovative device for

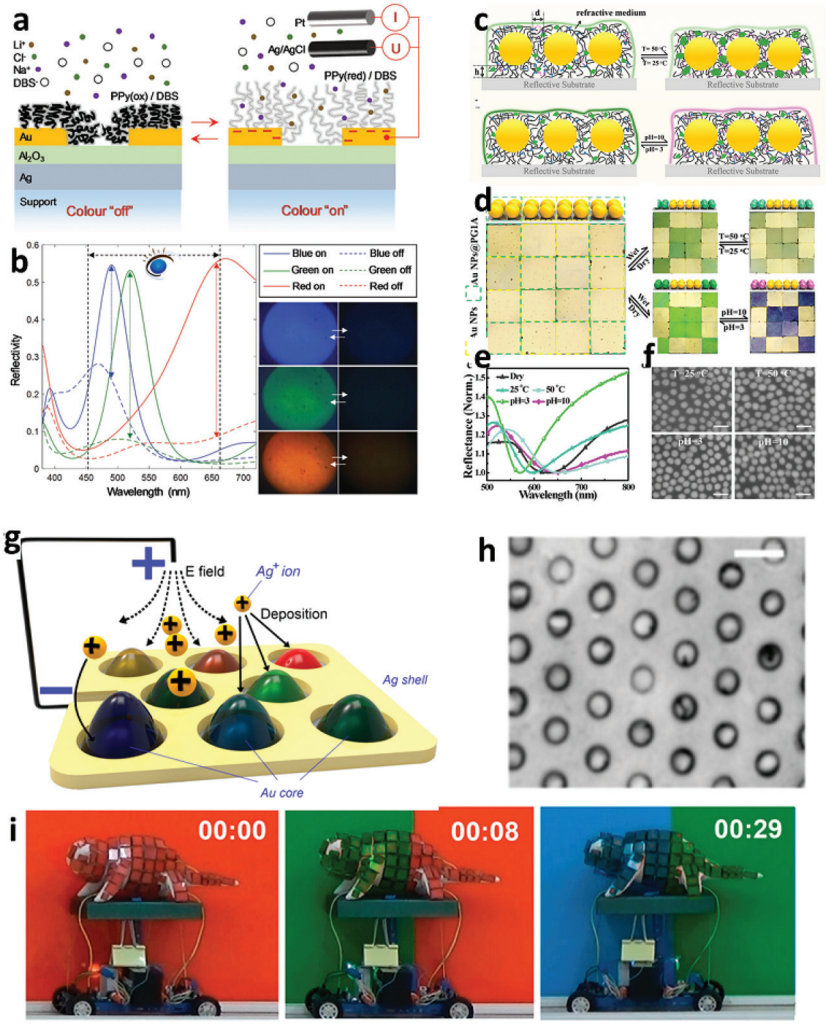

Fig. 17 The 2D plasmonic pigment for colorful switched dynamic discoloration:[44] (a) schematic representation of reflection modulation by inducing the conductive polymer (polypyrrole); (b) the characterization of the dynamic discoloration behaviour by adjusting the oxidation and reduction switching of the conductive polymer; (c–f) pH and temperature dual-responsive plasmonic switches of Au NP monolayers:[268] (c) the proposed thermo-triggered conformational change mechanism for the dynamic discoloration of the dendrimer coated Au NP monolayers on silicon wafer; (d) multiple-coded anticounterfeit labels. The labels were made up with multiple blocks of the dendrimer coated Au NP monolayer functionalized silicon wafers under different conduction pathways; UV-vis reflectance spectrum (e) and SEM characterization (f) of the dendrimer coated Au NP monolayers under different conduction pathways; (g–i) dynamic real-time plasmonic discoloration:[269] (g) schematic diagram of the dynamic real-time plasmonic discoloration device that consisted of Ag–Au NP arrays with controllable Ag shell thicknesses; (f) SEM image of the Au nanodome array. Scale bar: 100 nm; (i) the real-time monitoring of the plasmonic discoloration device; the instantaneous discoloration was achieved by the electric field regulating the electrodeposition time of Ag^{+}.

information storage with bright colors by using near-percolation metal films atop dielectric-metal sandwiches. Without preformed nanostructures, the bright colors can be acquired by reshaping the 4 nm Au NP islands after illumination with different laser power levels (Fig. 18i–k). Additionally, besides the ability of 2D MFGS of capturing light itself, synergistically enhancing light absorption is also an effective approach for information storage. Ding and co-workers gained fluorescence information storage by producing a Au cubic assembly enhanced QD system with the assistance of photolithography (Fig. 18l).[43]

5.4 Electrical applications

The functionalized 2D MFGS often presented prominent electrical conductivity. It is worth noting that the free-standing and macroscopic 2D MFGS have great electrical applications. Additionally, there is a growing demand for portable electronic devices in the modern age of digital information.

5.4.1 electrochemical detection. The 2D MFGS based electrochemical sensors are often referred to as chemiresistors, and the detection sensitivity is reflected in the changes of resistance values. Numerous studies have been conducted on 2D

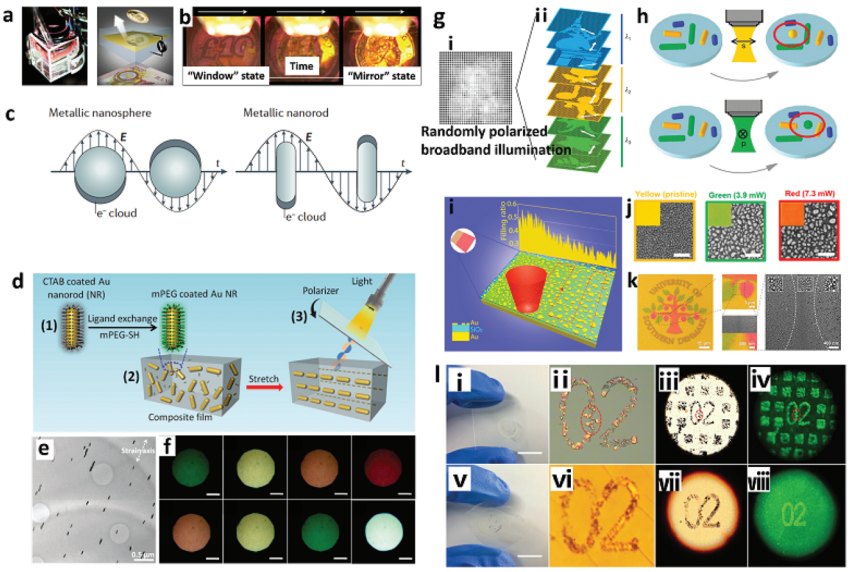

Fig. 18 (a and b) The information storage device by generating a liquid window–mirror with a controllable distance between Au NPs:[175] gradually emerging information by forming Au NP monolayers: from the "window" state to the "mirror" state; (c) surface-plasmon resonances of Au NPs with different shapes;[276] (d–f) the polarization dependent optical displays of Au NR films:[274] (d) schematic representation of the process (e) the TEM images of the hybrid film containing mPEG-capped Au NRs after stretching; (f) optical microscopy images of the stretched Au NR/PVA hybrid film with and without polarized light illumination with different angles; (g and h) a five-dimensional optical recording system by reshaping of disordered Au NRs:[277] (g) the collection of all patterns before (i) and after (ii) being read out by choosing the right polarization and wavelength; (h) schematic illustration of the reading mechanism: the linear polarized laser pulse should drastically match the Au NRs, which are aligned to the laser light polarization, and the absorption cross-section should match the laser wavelength; (i–l) multicolor information display by utilizing near-percolation metal films atop dielectric-metal sandwiches:[278] (i) schematic of the coloration mechanism. The reshaping of gold islands induced by the laser pulse in the sandwiches is the foundation of coloration; (j) SEM images of the 4 nm Au island structures in the sandwiches before (yellow) and after laser writing with different power levels (green and red). Scale bars: 100 nm. (k) Color writing with circularly polarized light. Bright field optical microscopy of images of the pattern written under circularly polarized light and read with unpolarized light and stepwise enlarged optical microscopy images and SEM images. (l) Optical information storage with Au NP array enhanced fluorescence:[43] sample fabricated on a glass substrate (i–iv) and on a flexible substrate (v–viii) with the assistance of photolithography and self-assembly.

MFGS based chemiresistors since the first work on chemiresistors, which was reported by Wohltjen and Snow.[279] The sensing (or conducting) mechanism of 2D MFGS is the thermally activated charge transport route, according to the following equation:[280,281]

$$\frac{\Delta R}{R_0} = e^{\beta\Delta\delta} \times e^{\Delta E_a/kT} - 1 \quad (5)$$

$\Delta R/R_0$ is the sensor response recorded as the relative resistance change, β is the tunnelling decay constant, δ is the distance between neighbouring Au NP cores, k is the Boltzmann constant, and T is the temperature.

Here, the two exponential terms represented the tunnelling of charges between neighbouring Au NPs and the thermal activation of charge transport, respectively. The activation energy (E_a) is usually produced by the Coulomb charging,[282] which would decrease with the increase of the particle distance between neighbouring Au NPs (δ), and would increase with the permittivity the Au NPs.[283] Thus, when the sorption of the analyte within the film occurred, the swelling of the film resulted in the increase of the relative resistance. Additionally, the analytes with the higher permittivity often result in the decrease of resistance.[284] According to this sensing principle, 2D MFGS based chemiresistors were used in various fields such as environmental detection.[87,285–287] They often presented some notable superiorities such as high sensitivity, rapid responsiveness and low power consumption.[282] For example, Olichwer and co-workers[284] constructed a chemiresistor that consisted of cross-linked Au NPs and a polyethylene (PE) flexible substrate (Fig. 19a–d). The sensitive response of resistance to the absorption of a small molecular organic vapor was monitored due to the dominant swelling function. The sensitivity of the proposed chemiresistors can be enhanced by inducing moderate tensile strain. This can be ascribed to the reversible rupture of the Au NP network and crack formation. This increased the freedom of the films and led to swelling in the lateral direction. In addition, the 2D MFGS based chemiresistors are also of great importance in some advanced applications such as health monitoring and biomedical diagnostics.[261,288] The disease-specific volatile organic compounds (VOCs) often shows significant differences between normal and cancerous tissues.[289,290] Much effort has been devoted by Haick's group to detect the VOCs in patients exhaled gases.[146,291] Besides a similar sensing mechanism to those of traditional chemiresistors, some special flexible substrates were utilized in the system to achieve optimized detec-

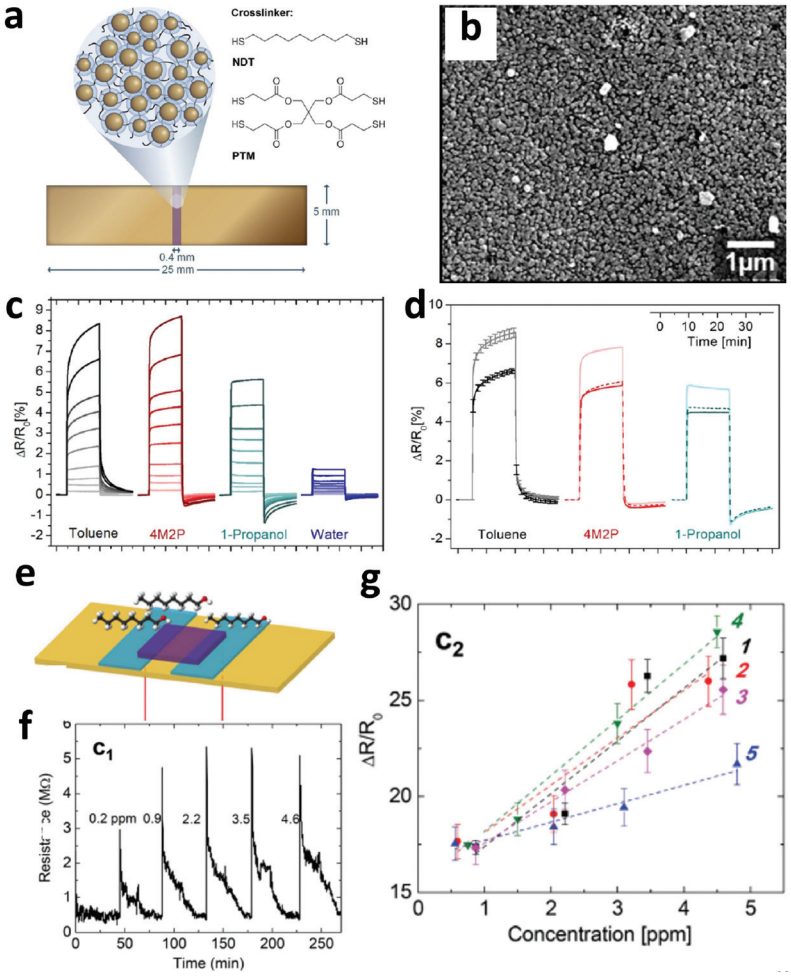

Fig. 19 (a–d) Ultrasensitive strain and vapor detection based on 2D cross-linked Au NP monolayers on polyethylene:[284] (a) schematic diagram of the 2D MFGS based resistor; (b) SEM images of the 2D cross-linked Au NP monolayer; (c) the response transients of the 2D MFGS based resistor to various solvent vapors; (d) response transients of the film under no strain (dark solid lines), under 1% strain (light solid lines), remeasured under no strain (dark dashed lines) to different solvent vapors; (e–g) construction of a 2D MFGS based flexible and self-healing sensing platform for VOC detection:[292] (e) schematic of the self-healing chemiresistor under VOC exposure; resistance responses (f) and calibration plots (g) of the relative resistance response of the 2D AuNP film chemiresistor under different conditions: bending experiments before and after electrode-cut and (electrode and AuNP)-cut.

tion performances. For example, self-healing chemiresistors for monitoring pressure, strain, temperature, and VOCs have been reported by compositing 2D MFGS with disulfide-cross-linked polyurethane (Fig. 19e–g).[292] The combination of high sensitivity and the self-healing property makes it possible to apply them under normal or harsh conditions.

5.4.2 Electronic skin. The so-called electronic skin (e-skin) is a system that makes robots feel like humans. Most potential applications of the e-skin are inspired by human skin, such as artificial prosthetics, wearable devices, health monitoring devices and smart robots.[293–296] Bao's group initiated the investigation of e-skin and has devoted much effort to e-skin for many years.[293,295,297] Generally, the e-skin is composed of two parts: a sensor and an electronic circuit. In detail, the sensing part is of vital importance that makes the e-skin perceive like human skin. The electronic circuit converts the perceived signals into information that our brains can understand. The working mechanism of e-skin is carried out, according to the theoretical investigation for the resistivity changes in 2D MFGS by Zellers' group.[298] However, similar to the optical sensors, e-skin usually requires supersensitivity and wide detection windows for detecting stran from skin.[147,155] Human skin motions include both subtle and large scale motions, such as subtle signals of artery pulses beating and large scale motions of joint bending.

Thus, most of the recent research studies have been conducted to design skin-imitating stretchable strain sensors with high sensitivity.[91,296] As a component of high mechanical flexibility and notable conductivity, ultrathin Au NWs become considerably attractive for e-skin.[299,300] Chen's group has explored many different flexible electronic sensors by using Au NWs.[46,301,302] For instance, they constructed Au NW based e-skin by combining them with an elastomeric substrate

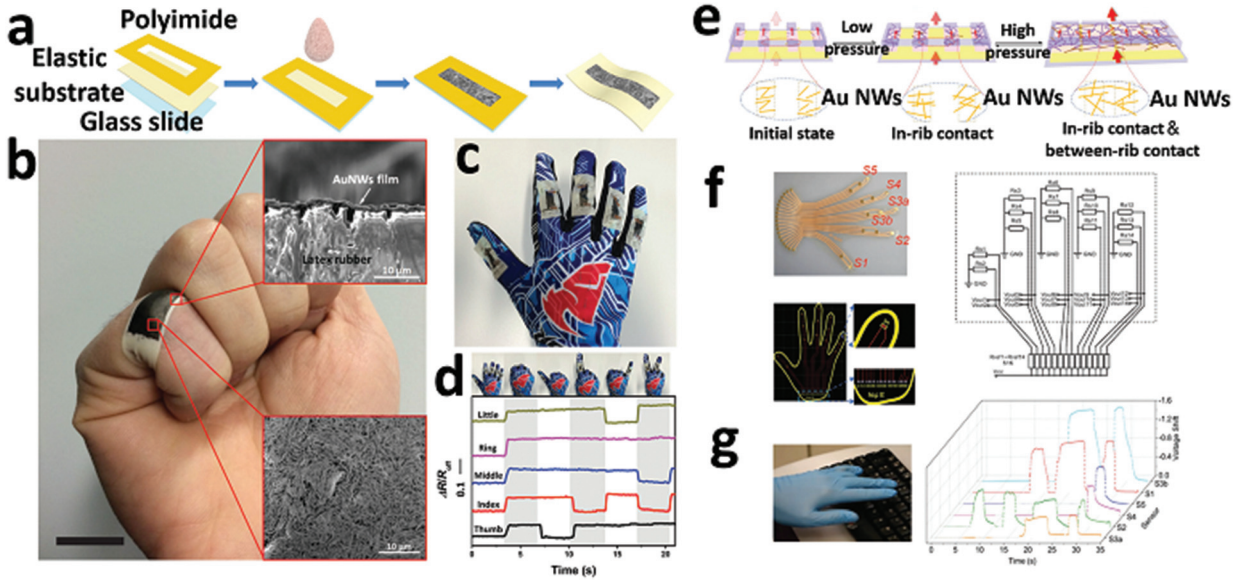

Fig. 20 (a–d) Wearable biomedical sensors based on 2D Au NW-elastic substrate composites:[155] (a) schematic diagram of the fabrication process of the e-skin; (b) photographs of the strain sensor ring attached on the little finger while bending. The scale bar is 1 cm; (c) photograph of a glove with the strain sensor attached on each finger; (d) resistance change by changing time for strain sensors on the glove at six different hand positions; (e–g) wearable pressure sensors based on ordered Au NW-hydrogel composites:[304] (e) schematic diagram of the working mechanism based on the bimodal contact mode of Au NWs: the microrib structures make the 2D composites possess wide strain detecting ranges; (f) photograph and the electrical circuit of the E-hand skin integrated with six pressure sensors and the electric design and a photograph of a human hand with the E-hand skin for detection; and (g) the measured signals of the different sensors in the E-hand skin.

(Fig. 20a–d).[155] The e-skin showed notable stretching ability, a rapid response time and high durability. More importantly, the e-skin presented dynamic tensile strain detecting properties in a range from 0.01% to 200%. Elastic hydrogels often had distinct mechanical and stimulus-responsive properties.[303] Yin and co-workers[304] utilized Au NWs and polyacrylamide hydrogels for wearable pressure sensors (Fig. 20e–g). The bimodal contact mode of Au NWs makes the wearable sensor exhibit high sensitivity and a wide detection range.

6. Summary and outlook

In this review, we have summarized the recent progress of macroscopic two-dimensional Au NP monolayer films including construction, functionalization and applications. The macroscopic and controllable Au NP monolayer films have been constructed *via* a series of methods such as interfacial assembly (gas–liquid, liquid–liquid, and gas–liquid–solid). The functionalization of the 2D MFGS also has been discussed for enhancing conductivity, increasing the stability and improving the optical properties. The applications of 2D MFGS, especially in optical and electrical detection, and optical and electrical devices, were summarized. Despite the impressive recent advances of 2D MFGS, there are challenges and opportunities in this field.

Primarily, there is still an urgent need to develop a universal and general approach to large-scale and repeated fabrication of uniform, particle gap-size controllable, excellent free-standing and easily transferable macroscopic 2D MFGS. For instance, most interfacial assembly approaches are susceptible to interference (atmospheric pressure, vibration, and humidity), which makes it difficult to obtain 2D MFGS with high uniformity. In addition, 2D MFGS with controllable gaps are extremely difficult to obtain, which tremendously hinders the application of 2D MFGS in various fields.

Another big issue is the limitations of the interfacial assembly method itself. For example, the air–liquid–solid system is unable to obtain free-standing monolayer films without substrates. To this end, some approaches to achieve accurately controllable 2D MFGS should be constructed.

Secondly, surface functional engineering should be more diversified. In the current studies, the function of 2D MFGS mainly focuses on LSPR sensors, SERS, catalysis and electrochemistry. For example, combining 2D MFGS with smart response polymers would endow 2D MFGS with intelligent response performance. Additionally, regulating 2D MFGS with proteins should increase the stability and biocompatibility of 2D MFGS.

Thirdly, wearable devices with lightweight, flexible, intelligent and efficient features will bring changes and development in the future. However, the application of 2D MFGS in flexible wearable devices is extremely limited except that Au NWs are widely used. Thus, broadening the application of functional 2D MFGS in flexible wearable devices is a very promising direction.

Ultimately, bioelectronics using 2D MFGS should be a significant field. Organism membranes possess special structures (for example, interlocked dermal epidermal layers) that make it possible to achieve body monitoring. The functional 2D MFGS with high stretchability, conformability, stability, and certain mechanical strength satisfy the demands of bioelectronic applications. But, there is still a long way to go for human health monitoring with functional 2D MFGS.

The abovementioned challenges in the field of 2D MFGS need mutual efforts from interdisciplinary experts with different backgrounds. We believe that there will be vigorous development in 2D MFGS monolayer films in near future.

Conflicts of interest

There are no conflicts to declare.

Acknowledgements

We gratefully acknowledge the Natural Science Foundation of China (Grant 51873222), Fujian province-Chinese Academy of Sciences STS project (2017T31010024), and Youth Innovation Promotion Association of Chinese Academy of Science (2016268).

Notes and references

1 E. C. Dreaden, A. M. Alkilany, X. Huang, C. J. Murphy and M. A. El-Sayed, *Chem. Soc. Rev.*, 2012, **41**, 2740–2779.
2 K. C. Ng, I. D. Rukhlenko, Y. Chen, Y. Tang, M. Premaratne and W. Cheng, *ACS Nano*, 2012, **6**, 925–934.
3 X. Lu, Y. Huang, B. Liu, L. Zhang, L. Song, J. Zhang, A. Zhang and T. Chen, *Chem. Mater.*, 2018, **30**, 1989–1997.
4 P. Cardenas, C. Kong, J. He, S. Litvin, M. L. Meyerson and Z. Nie, *ACS Nano*, 2018, **12**, 1107–1119.
5 Y. Shin, J. Song, D. Kim and T. Kang, *Adv. Mater.*, 2015, **27**, 4344–4350.
6 S. T. Jones, J. M. Zayed and O. A. Scherman, *Nanoscale*, 2013, **5**, 5299–5302.
7 F. C. Leung, S. Y. Leung, C. Y. Chung and V. W. Yam, *J. Am. Chem. Soc.*, 2016, **138**, 2989–2992.
8 Y. Wang, Y. F. Li, J. Wang, Y. Sang and C. Z. Huang, *Chem. Commun.*, 2010, **46**, 1332–1334.
9 D. A. Walker, C. E. Wilmer, B. Kowalczyk, K. J. Bishop and B. A. Grzybowski, *Nano Lett.*, 2010, **10**, 2275–2280.
10 C. Zhang, E. You, Q. Jin, Y. Yuan, M. Xu, S. Ding, J. Yao and Z. Tian, *Chem. Commun.*, 2017, **53**, 6788–6791.
11 N. Kwon, H. Oh, R. Kim, A. Sinha, J. Kim, J. Shin, J. W. M. Chon and B. Lim, *Nano Lett.*, 2018, **18**, 5927–5932.
12 L. Zhang, P. Xiao, W. Lu, J. Zhang, J. Gu, Y. Huang and T. Chen, *Adv. Mater. Interfaces*, 2016, **3**, 1600170.
13 P. P. E. Smirnov, M. D. Scanlon and H. H. Girault, *ACS Nano*, 2015, **6**, 6565–6575.
14 E. Smirnov, P. Peljo and H. H. Girault, *Chem. Commun.*, 2017, **53**, 4108–4111.
15 L. Zhang, X. Zha, G. Zhang, J. Gu, W. Zhang, Y. Huang, J. Zhang and T. Chen, *J. Mater. Chem. A*, 2018, **6**, 10217–10225.
16 Y. Xu, M. P. Konrad, J. L. Trotter, C. P. McCoy and S. E. Bell, *Small*, 2017, **13**, 1602163.
17 S. Si, W. Liang, Y. Sun, J. Huang, W. Ma, Z. Liang, Q. Bao and L. Jiang, *Adv. Funct. Mater.*, 2016, **26**, 8137–8145.
18 Z. Guo, Y. Jia, X. Song, J. Lu, X. Lu, B. Liu, J. Han, Y. Huang, J. Zhang and T. Chen, *Anal. Chem.*, 2018, **90**, 6124–6130.
19 P. Fang, H. Deng, M. D. Scanlon, F. Gumy, H. J. Lee, D. Momotenko, V. Amstutz, F. C. Salazar, C. M. Pereira, Z. Yang and H. H. Girault, *ACS Nano*, 2013, **10**, 9241–9248.
20 J. Kim, M. Lee, C. Song, J.-K. Song, J. Koo, D. Lee, H. Shim, J. Kim, M. Lee, T. Hyeon and D. Kim, *Sci. Adv.*, 2016, **2**, e1501101.
21 Y. Liu, S. Yu, R. Feng, A. Bernard, Y. Liu, Y. Zhang, H. Duan, W. Shang, P. Tao, C. Song and T. Deng, *Adv. Mater.*, 2015, **27**, 2768–2774.
22 K. Bae, G. Kang, S. K. Cho, W. Park, K. Kim and W. J. Padilla, *Nat. Commun.*, 2015, **6**, 10103.
23 K. Zhang, J. Zhao, J. Ji, Y. Li and B. Liu, *Anal. Chem.*, 2015, **87**, 8702–8708.
24 M. Nguyen, N. Felidj and C. Mangeney, *Chem. Mater.*, 2016, **28**, 3564–3577.
25 M. Yanagisawa, C. Watanabe and K. Fujiwara, *Gels*, 2018, **4**, 29.
26 T. S. Sreeprasad and T. Pradeep, *Langmuir*, 2011, **27**, 3381–3390.
27 A. Lukach, K. Liu, H. Therien-Aubin and E. Kumacheva, *J. Am. Chem. Soc.*, 2012, **134**, 18853–18859.
28 A. Petukhova, J. Greener, K. Liu, D. Nykypanchuk, R. Nicolay, K. Matyjaszewski and E. Kumacheva, *Small*, 2012, **8**, 731–737.
29 T. Wang, J. Lynch, O. Chen, Z. Wang, X. Wang, D. LaMontagne, H. Wu, Z. Wang and Y. C. Cao, *Science*, 2012, **338**, 358–363.
30 R. A. Alvarez-Puebla, A. Agarwal, P. Manna, B. P. Khanal, P. Aldeanueva-Potel, E. Carbo-Argibay, N. Pazos-Perez, L. Vigderman, E. R. Zubarev, N. A. Kotov and L. M. Liz-Marzan, *Proc. Natl. Acad. Sci. U. S. A.*, 2011, **108**, 8157–8161.
31 M. Zanella, R. Gomes, M. Povia, C. Giannini, Y. Zhang, A. Riskin, M. Van Bael, Z. Hens and L. Manna, *Adv. Mater.*, 2011, **23**, 2205–2209.
32 V. Liberman, C. Yilmaz, T. M. Bloomstein, S. Somu, Y. Echegoyen, A. Busnaina, S. G. Cann, K. E. Krohn, M. F. Marchant and M. Rothschild, *Adv. Mater.*, 2010, **22**, 4298–4302.
33 X. Wang, L. Meng, K. Lin, J. Feng, T. Huang, Z. Yang and B. Ren, *ACS Nano*, 2014, **8**, 528–536.

34 E. Smirnov, D. Momotenko, H. Vrubel, M. A. Méndez, P.-F. Brevet and H. H. Girault, *ACS Nano*, 2014, **8**, 9471–9481.
35 N. Yan, X. Liu, J. Zhu, Y. Zhu and W. Jiang, *ACS Nano*, 2019, **13**, 6638–6646.
36 v. S. l.-S. a. B. Vlčkova, *Nano Lett.*, 2002, **2**, 121–125.
37 Y.-K. Park and S. Park, *Chem. Mater.*, 2008, **20**, 2388–2393.
38 X. Wang, X. Zhu, H. Shi, Y. Chen, Z. Chen, Y. Zeng, Z. Tang and H. Duan, *ACS Appl. Mater. Interfaces*, 2018, **10**, 35607–35614.
39 C. Wang, X. Wu, P. Dong, J. Chen and R. Xiao, *Biosens. Bioelectron.*, 2016, **86**, 944–950.
40 L. Hu, M. Chen, X. Fang and L. Wu, *Chem. Soc. Rev.*, 2012, **41**, 1350–1362.
41 K. Wang, H. Ling, Y. Bao, M. Yang, Y. Yang, M. Hussain, H. Wang, L. Zhang, L. Xie, M. Yi, W. Huang, X. Xie and J. Zhu, *Adv. Mater.*, 2018, **30**, 1800595.
42 A. A. K. Joshua, B. Edel and M. Urbakh, *ACS Nano*, 2013, **7**, 9526–9532.
43 Y. Ding, Y. You, Y. Sang, Y. Wang, M. Zhao, C. Liang, C. Lu, D. Liu, J. Zhou, Z. Tang and J. Shi, *Adv. Opt. Mater.*, 2017, **5**, 1700551.
44 K. Xiong, G. Emilsson, A. Maziz, X. Yang, L. Shao, E. W. Jager and A. B. Dahlin, *Adv. Mater.*, 2016, **28**, 9956–9960.
45 L. Shao, X. Zhuo and J. Wang, *Adv. Mater.*, 2018, **30**, e1704338.
46 Y. Wang, S. Gong, S. J. Wang, X. Yang, Y. Ling, L. W. Yap, D. Dong, G. P. Simon and W. Cheng, *ACS Nano*, 2018, **12**, 9742–9749.
47 Y. Wang, S. Gong, D. Gomez, Y. Ling, L. W. Yap, G. P. Simon and W. Cheng, *ACS Nano*, 2018, **12**, 8717–8722.
48 G. Gonzalez-Rubio, A. Guerrero-Martinez and L. M. Liz-Marzan, *Acc. Chem. Res.*, 2016, **49**, 678–686.
49 M. Grzelczak, L. M. Liz-Marzan and R. Klajn, *Chem. Soc. Rev.*, 2019, **48**, 1342–1361.
50 S. K. Ghosh and T. Pal, *Chem. Rev.*, 2007, **107**, 4797–4862.
51 C. Vericat, M. E. Vela, G. Benitez, P. Carro and R. C. Salvarezza, *Chem. Soc. Rev.*, 2010, **39**, 1805–1834.
52 S. Y. Zhang, M. D. Regulacio and M. Y. Han, *Chem. Soc. Rev.*, 2014, **43**, 2301–2323.
53 L. Srisombat, A. C. Jamison and T. R. Lee, *Colloids Surf., A*, 2011, **390**, 1–19.
54 W. Wei and G. Ge, *Part. Part. Syst. Charact.*, 2013, **30**, 837–841.
55 P. Pieranski, *Phys. Rev. Lett.*, 1980, **45**, 569–572.
56 B. P. B. Vesselin, N. Paunov and N. P. Ashby, *Langmuir*, 2002, **18**, 6946–6955.
57 L. Huo, W. Li, L. Lu, H. Cui, S. Xi, J. Wang, B. Zhao, Y. Shen and Z. Lu, *Chem. Mater.*, 2000, **12**, 790–794.
58 B. P. Binks, *Curr. Opin. Colloid Interface Sci.*, 2002, **7**, 21–41.
59 L. Xu, G. Han, J. Hu, Y. He, J. Pan, Y. Li and J. Xiang, *Phys. Chem. Chem. Phys.*, 2009, **11**, 6490–6497.
60 J. Hu, G. Han, B. Ren, S. Sun and Z. Tian, *Langmuir*, 2004, **20**, 8831–8838.
61 J. Hu, B. Zhao, W. Xu, Y. Fan, B. Li and Y. Ozaki, *J. Phys. Chem. B*, 2002, **106**, 6500–6506.
62 L. Wang, Y. Zhu, L. Xu, W. Chen, H. Kuang, L. Liu, A. Agarwal, C. Xu and N. A. Kotov, *Angew. Chem., Int. Ed.*, 2010, **49**, 5472–5475.
63 Y. R. Zhang, Y. Z. Xu, Y. Xia, W. Huang, F. A. Liu, Y. C. Yang and Z. L. Li, *J. Colloid Interface Sci.*, 2011, **359**, 536–541.
64 Y. Liu, Y. Liu, P. Tao, W. Shang, C. Song and T. Deng, *Nanoscale*, 2014, **6**, 14662–14666.
65 Z. Wang, Y. Liu, P. Tao, Q. Shen, N. Yi, F. Zhang, Q. Liu, C. Song, D. Zhang, W. Shang and T. Deng, *Small*, 2014, **10**, 3234–3239.
66 W. Wei and G. Ge, *Part. Part. Syst. Charact.*, 2013, **30**, 837–841.
67 B. Kim, S. L. Tripp and A. Wei, *J. Am. Chem. Soc.*, 2001, **123**, 7955–7956.
68 T. Ming, X. Kou, H. Chen, T. Wang, H.-L. Tam, K.-W. Cheah, J.-Y. Chen and J. Wang, *Angew. Chem., Int. Ed.*, 2008, **47**, 9685–9690.
69 S. Kundu, *Langmuir*, 2011, **27**, 3930–3936.
70 K. E. Mueggenburg, X. M. Lin, R. H. Goldsmith and H. M. Jaeger, *Nat. Mater.*, 2007, **6**, 656–660.
71 F. Kim, S. Kwan, J. Akana and P. Yang, *J. Am. Chem. Soc.*, 2001, **123**, 4360–4361.
72 D. Liu, C. Li, F. Zhou, T. Zhang, G. Liu, W. Cai and Y. Li, *Adv. Mater. Interfaces*, 2017, 1600976.
73 I. Kosif, K. Kratz, S. S. You, M. K. Bera, K. Kim, B. Leahy, T. Emrick, K. Y. Lee and B. Lin, *ACS Nano*, 2017, **11**, 1292–1300.
74 D. Liu, C. Li, F. Zhou, T. Zhang, G. Liu, W. Cai and Y. Li, *Adv. Mater. Interfaces*, 2017, 1600976.
75 X. Ye, J. Chen, D. C. Reifsnyder, C. Zheng and B. Murray, *Nano Lett.*, 2013, **13**, 2163–2171.
76 J. Chen, Y. Huang, P. Kannan, L. Zhang, Z. Lin, J. Zhang, T. Chen and L. Guo, *Anal. Chem.*, 2016, **88**, 2149–2155.
77 P. Wang, L. Wu, Z. Lu, Q. Li, W. Yin, F. Ding and H. Han, *Anal. Chem.*, 2017, **89**, 2424–2431.
78 J. J. Armao Iv, I. Nyrkova, G. Fuks, A. Osypenko, M. Maaloum, E. Moulin, R. Arenal, O. Gavat, A. Semenov and N. Giuseppone, *J. Am. Chem. Soc.*, 2017, **139**, 2345–2350.
79 C. Niu, B. Zou, Y. Wang, L. Cheng, H. Zheng and S. Zhou, *Langmuir*, 2016, **32**, 858–863.
80 B. Zhou, M. Mao, X. Cao, M. Ge, X. Tang, S. Li, D. Lin, L. Yang and J. Liu, *Anal. Chem.*, 2018, **90**, 3826–3832.
81 H. Duan, D. Wang, D. G. Kurth and H. Mohwald, *Angew. Chem., Int. Ed.*, 2004, **43**, 5639–5642.
82 J. F. Li, Y. F. Huang, Y. Ding, Z. L. Yang, S. B. Li, X. S. Zhou, F. R. Fan, W. Zhang, Z. Y. Zhou, D. Y. Wu, B. Ren, Z. L. Wang and Z. Q. Tian, *Nature*, 2010, **464**, 392–395.
83 K. Liu, Y. Bai, L. Zhang, Z. Yang, Q. Fan, H. Zheng, Y. Yin and C. Gao, *Nano Lett.*, 2016, **16**, 3675–3681.

84 G. Lu, H. Li and H. Zhang, *Small*, 2012, **8**, 1336–1340.
85 A. Tittl, X. Yin, H. Giessen, X. D. Tian, Z. Q. Tian, C. Kremers, D. N. Chigrin and N. Liu, *Nano Lett.*, 2013, **13**, 1816–1821.
86 J. F. Li, S. Y. Ding, Z. L. Yang, M. L. Bai, J. R. Anema, X. Wang, A. Wang, D. Y. Wu, B. Ren, S. M. Hou, T. Wandlowski and Z. Q. Tian, *J. Am. Chem. Soc.*, 2011, **133**, 15922–15925.
87 Y. Joseph, I. Besnard, M. Rosenberger, B. Guse, H.-G. Nothofer, J. M. Wessels, U. Wild, A. K.-Gericke, D. Su, R. Schlogl, A. Yasuda and T. Vossmeyer, *J. Phys. Chem. B*, 2003, **107**, 7406–7413.
88 J. F. Li, Y. J. Zhang, S. Y. Ding, R. Panneerselvam and Z. Q. Tian, *Chem. Rev.*, 2017, **117**, 5002–5069.
89 X. Zhang, Y. Zhu, X. Yang, Y. Zhou, Y. Yao and C. Li, *Nanoscale*, 2014, **6**, 5971–5979.
90 J. Jiang, S. Zou, L. Ma, S. Wang, J. Liao and Z. Zhang, *ACS Appl. Mater. Interfaces*, 2018, **10**, 9129–9135.
91 Y. Yang, H. Zhang, Z.-H. Lin, Y. Zhou, Q. Jing, Y. Su, J. Yang, J. Chen, C. Hu and Z. Wang, *ACS Nano*, 2013, **7**, 9213–9222.
92 X. Li, H. Hu, D. Li, Z. Shen, Q. Xiong, S. Li and H. J. Fan, *J. Phys. Chem. C*, 2010, **114**, 11040–11049.
93 L. Tian, M. Su, F. Yu, Y. Xu, X. Li, L. Li, H. Liu and W. Tan, *Nat. Commun.*, 2018, **9**, 3642.
94 P. Miao, T. Liu, X. Li, L. Ning, J. Yin and K. Han, *Biosens. Bioelectron.*, 2013, **49**, 20–24.
95 M. Mohan, N. Mohan and D. Chand, *J. Mater. Chem. A*, 2015, **3**, 21167–21177.
96 W. A. Ducker and T. J. Senden, *Langmuir*, 1992, **8**, 1831–1836.
97 T. Kim, K. Lee, M. Gong and S.-W. Joo, *Langmuir*, 2005, **21**, 9524–9528.
98 A. Wei, *Chem. Commun.*, 2006, 1581–1591.
99 S. Shi and T. P. Russell, *Adv. Mater.*, 2018, **30**, e1800714.
100 J. W. Liu, S. Y. Zhang, H. Qi, W. C. Wen and S. H. Yu, *Small*, 2012, **8**, 2412–2420.
101 R. Dong, T. Zhang and X. Feng, *Chem. Rev.*, 2018, **118**, 6189–6235.
102 M. D. Scanlon, E. Smirnov, T. J. Stockmann and P. Peljo, *Chem. Rev.*, 2018, **118**, 3722–3751.
103 Y.-K. Park, S.-H. Yoo and S. Park, *Langmuir*, 2007, **23**, 10505–10510.
104 G. Yang and D. T. Hallinan, *Sci. Rep.*, 2016, **6**, 35339.
105 E. S. Shibu, J. Cyriac, T. Pradeep and J. Chakrabarti, *Nanoscale*, 2011, **3**, 1066–1072.
106 X. Lu, Y. Huang, B. Liu, L. Zhang, L. Song, J. Zhang, A. Zhang and T. Chen, *Chem. Mater.*, 2018, **30**, 1989–1997.
107 C. G. S. Vartash and E. Rabani, *J. Phys. Chem. C*, 2010, **114**, 11040–11049.
108 M. V. Kovalenko, M. Scheele and D. V. Talapin, *Science*, 2009, **324**, 1417–1420.
109 L. Xu, W. Ma, L. Wang, C. Xu, H. Kuang and N. A. Kotov, *Chem. Soc. Rev.*, 2013, **42**, 3114–3126.
110 M. Anyfantakis and D. Baigl, *Angew. Chem., Int. Ed.*, 2014, **53**, 14077–14081.
111 R. Deegan, O. Bakajin, T. Dupont, G. Huber, S. Nagel and T. Witten, *Nature*, 1997, **389**, 827.
112 D. Zhang, B. Ma, L. Tang and H. Liu, *Anal. Chem.*, 2018, **90**, 1482–1486.
113 A. L. Marsico, B. Duncan, R. F. Landis, G. Y. Tonga, V. M. Rotello and R. W. Vachet, *Anal. Chem.*, 2017, **89**, 3009–3014.
114 J. Sun, B. Bao, M. He, H. Zhou and Y. Song, *ACS Appl. Mater. Interfaces*, 2015, **7**, 28086–28099.
115 A. Dong, J. Chen, S. J. Oh, W. K. Koh, F. Xiu, X. Ye, D. K. Ko, K. L. Wang, C. R. Kagan and C. B. Murray, *Nano Lett.*, 2011, **11**, 841–846.
116 T. Ming, X. Kou, H. Chen, T. Wang, H. L. Tam, K. W. Cheah, J. Y. Chen and J. Wang, *Angew. Chem., Int. Ed.*, 2008, **47**, 9685–9690.
117 X. Shen, C.-M. Ho and T.-S. Wong, *J. Phys. Chem. B*, 2010, **114**, 5269–5274.
118 P. Li, Y. Li, Z. K. Zhou, S. Tang, X. F. Yu, S. Xiao, Z. Wu, Q. Xiao, Y. Zhao, H. Wang and P. K. Chu, *Adv. Mater.*, 2016, **28**, 2511–2517.
119 P. J. Yunker, T. Still, M. A. Lohr and A. G. Yodh, *Nature*, 2011, **476**, 308–311.
120 T. Ming, X. Kou, H. Chen, T. Wang, H. L. Tam, K. W. Cheah, J. Y. Chen and J. Wang, *Angew. Chem., Int. Ed.*, 2008, **47**, 9685–9690.
121 X. Shen, C.-M. Ho and T.-S. Wong, *J. Phys. Chem. B*, 2010, **114**, 5269–5274.
122 L. E. Scriven and C. V. Sternling, *Nature*, 1960, **187**, 186–188.
123 M. Majumder, C. S. Rendall, J. A. Eukel, J. Y. Wang, N. Behabtu, C. L. Pint, T. Y. Liu, A. W. Orbaek, F. Mirri, J. Nam, A. R. Barron, R. H. Hauge, H. K. Schmidt and M. Pasquali, *J. Phys. Chem. B*, 2012, **116**, 6536–6542.
124 X. Shen, C.- M. Ho and T.-S. Wong, *J. Phys. Chem. B*, 2010, **114**, 5269–5274.
125 H. B. Eral and D. J. C. M. 't Mannetje, *Colloid Polym. Sci.*, 2012, **291**, 247–260.
126 M. Kuang, J. Wang, B. Bao, F. Li, L. Wang, L. Jiang and Y. Song, *Adv. Opt. Mater.*, 2014, **2**, 34–38.
127 R. D. Deegan, *Phys. Rev. E: Stat. Phys., Plasmas, Fluids, Relat. Interdiscip. Top.*, 2000, **61**, 475–485.
128 Y. Chen, Q. Xu, Y. Jin, X. Qian, L. Liu, J. Liu and V. Ganesan, *Macromolecules*, 2018, **51**, 4143–4157.
129 Q. Yang, M. Deng, H. Li, M. Li, C. Zhang, W. Shen, Y. Li, D. Guo and Y. Song, *Nanoscale*, 2015, **7**, 421–425.
130 Y. Rong, L. Song, P. Si, L. Zhang, X. Lu, J. Zhang, Z. Nie, Y. Huang and T. Chen, *Langmuir*, 2017, **33**, 13867–13873.
131 P. N. Sarkar and P. S, *J. Am. Chem. Soc.*, 1996, **79**, 1987–2002.
132 H. Zhang, J. Cadusch, C. Kinnear, T. James, A. Roberts and P. Mulvaney, *ACS Nano*, 2018, **12**, 7529–7537.
133 K. M. Baek, J. Kim, S. Kim, S. H. Cho, M. S. Jang, J. Oh and Y. S. Jung, *Chem. Mater.*, 2018, **30**, 6183–6191.
134 Y.-W. Wang, K.-C. Kao, J.-K. Wang and C.-Y. Mou, *J. Phys. Chem. C*, 2016, **120**, 24382–24388.

135 L. Chen, Y. Huang, L. Song, W. Yin, L. Hou, X. Liu and T. Chen, *ACS Appl. Mater. Interfaces*, 2019, **11**, 36259–36269.
136 S. Zeng, D. Baillargeat, H. P. Ho and K. T. Yong, *Chem. Soc. Rev.*, 2014, **43**, 3426–3452.
137 X. Yang, M. Yang, B. Pang, M. Vara and Y. Xia, *Chem. Rev.*, 2015, **115**, 10410–10488.
138 K. Ode, M. Honjo, Y. Takashima, T. Tsuruoka and K. Akamatsu, *ACS Appl. Mater. Interfaces*, 2016, **8**, 20522–20526.
139 C. J. Orendorff and C. J. Murphy, *J. Phys. Chem. B*, 2006, **110**, 3990–3994.
140 L. Wang, X. Shi, N. N. Kariuki, M. Schadt, G. R. Wang, Q. Rendeng, J. Choi, J. Luo, S. Lu and C.-J. Zhong, *J. Am. Chem. Soc.*, 2007, **129**, 2161–2170.
141 G. R. Wang, L. Wang, Q. Rendeng, J. Wang, J. Luo and C.-J. Zhong, *J. Mater. Chem.*, 2007, **17**, 457–462.
142 L. Wang, J. Luo, M. J. Schadt and C. J. Zhong, *Langmuir*, 2010, **26**, 618–632.
143 L. Han, M. M. Maye and C.-J. Zhong, *Anal. Chem.*, 2001, **73**, 4441–4449.
144 G. Yang, L. Hu, T. D. Keiper, P. Xiong and D. T. Hallinan, *Langmuir*, 2016, **32**, 4022–4033.
145 J. H. Maurer, L. Gonzalez-Garcia, B. Reiser, I. Kanelidis and T. Kraus, *Nano Lett.*, 2016, **16**, 2921–2925.
146 M. Segev-Bar, G. Konvalina and H. Haick, *Adv. Mater.*, 2015, **27**, 1779–1784.
147 B. Ketelsen, M. Yesilmen, H. Schlicke, H. Noei, C. H. Su, Y. C. Liao and T. Vossmeyer, *ACS Appl. Mater. Interfaces*, 2018, **10**, 37374–37385.
148 D. Coursault, N. Sule, J. Parker, Y. Bao and N. F. Scherer, *Nano Lett.*, 2018, **18**, 3391–3399.
149 S. Gong, W. Schwalb, Y. Wang, Y. Chen, Y. Tang, J. Si, B. Shirinzadeh and W. Cheng, *Nat. Commun.*, 2014, **5**, 3132.
150 C. Farcau, H. Moreira, B. Viallet, J. Grisolia, D. Ciuculescu-Pradines, C. Amiens and L. Ressier, *J. Phys. Chem. C*, 2011, **115**, 14494–14499.
151 S. Gong, D. T. Lai, Y. Wang, L. W. Yap, K. J. Si, Q. Shi, N. N. Jason, T. Sridhar, H. Uddin and W. Cheng, *ACS Appl. Mater. Interfaces*, 2015, **7**, 19700–19708.
152 A. Ostendorf, C. Cramer, G. Decher and M. Schönhoff, *J. Phys. Chem. C*, 2015, **119**, 9543–9549.
153 D. Lee, H. Lee, Y. Jeong, Y. Ahn, G. Nam and Y. Lee, *Adv. Mater.*, 2016, **28**, 9364–9369.
154 J. G. Simmons, *Phys. Rev.*, 1967, **155**, 657–660.
155 S. Gong, D. T. H. Lai, B. Su, K. J. Si, Z. Ma, L. W. Yap, P. Guo and W. Cheng, *Adv. Electron. Mater.*, 2015, **1**, 1400063.
156 Z. Yin, H. Li, W. Xu, S. Cui, D. Zhou, X. Chen, Y. Zhu, G. Qin and H. Song, *Adv. Mater.*, 2016, **28**, 2518–2525.
157 D. Y. Yun and T. W. Kim, *Carbon*, 2015, **88**, 26–32.
158 J.-W. Liu, W.-R. Huang, M. Gong, M. Zhang, J.-L. Wang, J. Zheng and S.-H. Yu, *Adv. Mater.*, 2013, **25**, 5910–5915.
159 Y. Liu, X. Han, L. He and Y. Yin, *Angew. Chem., Int. Ed.*, 2012, **51**, 6373–6377.
160 L. Dai, L. Song, Y. Huang, L. Zhang, X. Lu, J. Zhang and T. Chen, *Langmuir*, 2017, **33**, 5378–5384.
161 Y. Huang, L. Dai, L. Song, L. Zhang, Y. Rong, J. Zhang, Z. Nie and T. Chen, *ACS Appl. Mater. Interfaces*, 2016, **8**, 27949–27955.
162 Y. Jia, L. Zhang, L. Song, L. Dai, X. Lu, Y. Huang, J. Zhang, Z. Guo and T. Chen, *Langmuir*, 2017, **33**, 13376–13383.
163 M. Atighilorestani, H. Jiang and B. Kaminska, *Adv. Opt. Mater.*, 2018, **6**, 1801179.
164 W. Shao, Z. Liang, T. Guan, J. Chen, Z. Wang, H. Wu, J. Zheng, I. Abdulhalim and L. Jiang, *J. Mater. Chem. A*, 2018, **6**, 8419–8429.
165 R. Shenhar, T. B. Norsten and V. M. Rotello, *Adv. Mater.*, 2005, **17**, 657–669.
166 N. Kwon, H. Oh, R. Kim, A. Sinha, J. Kim, J. Shin, J. W. M. Chon and B. Lim, *Nano Lett.*, 2018, **18**, 5927–5932.
167 Z. Zhou, Y. Yu, N. Sun, H. Mohwald, P. Gu, L. Wang, W. Zhang, T. A. F. Konig, A. Fery and G. Zhang, *ACS Appl. Mater. Interfaces*, 2017, **9**, 35244–35252.
168 V. K. S. Hsiao, Y. B. Zheng, B. K. Juluri and T. J. Huang, *Adv. Mater.*, 2008, **20**, 3528–3532.
169 C. Matricardi, C. Hanske, J. L. Garcia-Pomar, J. Langer, A. Mihi and L. M. Liz-Marzan, *ACS Nano*, 2018, **12**, 8531–8539.
170 S. Lim, J. E. Song, J. A. La and E. C. Cho, *Chem. Mater.*, 2014, **26**, 3272–3279.
171 K. Vogele, J. List, G. Pardatscher, N. B. Holland, F. C. Simmel and T. Pirzer, *ACS Nano*, 2016, **10**, 11377–11384.
172 J. Qi, Y. Xiang, W. Yan, M. Li, L. Yang, Z. Chen, W. Cai, J. Chen, Y. Li, Q. Wu, X. Yu, Q. Sun and J. Xu, *J. Phys. Chem. C*, 2016, **120**, 24932–24940.
173 G. Yang, L. Hu, T. D. Keiper, P. Xiong and D. T. Hallinan Jr., *Langmuir*, 2016, **32**, 4022–4033.
174 J. W. Liu, W. R. Huang, M. Gong, M. Zhang, J. L. Wang, J. Zheng and S. H. Yu, *Adv. Mater.*, 2013, **25**, 5910–5915.
175 Y. Montelongo, D. Sikdar, Y. Ma, A. J. S. McIntosh, L. Velleman, A. R. Kucernak, J. B. Edel and A. A. Kornyshev, *Nat. Mater.*, 2017, **16**, 1127–1135.
176 J. B. Edel, A. A. Kornyshev, A. R. Kucernak and M. Urbakh, *Chem. Soc. Rev.*, 2016, **45**, 1581–1596.
177 C. Hanske, M. Tebbe, C. Kuttner, V. Bieber, V. V. Tsukruk, M. Chanana, T. A. Konig and A. Fery, *Nano Lett.*, 2014, **14**, 6863–6871.
178 Y. H. Jang, K. Chung, L. N. Quan, B. Špačková, H. Šípová, S. Moon, W. J. Cho, H.-Y. Shin, Y. J. Jang, J.-E. Lee, S. T. Kochuveedu, M. J. Yoon, J. Kim, S. Yoon, J. K. Kim, D. Kim, J. Homola and D. H. Kim, *Nanoscale*, 2013, **5**, 12261.
179 L. Wang, F. Montagne, P. Hoffmann, H. Heinzelmann and R. Pugin, *J. Colloid Interface Sci.*, 2011, **356**, 496–504.
180 W. Lee, S. Y. Lee, R. M. Briber and O. Rabin, *Adv. Funct. Mater.*, 2011, **21**, 3424–3429.

181 L. B. T. Catherine, J. Murphy, A. M. Alkilany, P. N. Sisco, S. P. Boulos, S. T. Sivapalan, J. An Yang, D. J. Chernak and J. Huang, *J. Phys. Chem. Lett.*, 2010, **1**, 2867–2975.
182 M. Nguyen, X. Sun, E. Lacaze, P. M. Winkler, A. Hohenau, J. R. Krenn, C. Bourdillon, A. Lamouri, J. Grand, G. Lévi, L. Boubekeur-Lecaque, C. Mangeney and N. Félidj, *ACS Photonics*, 2015, **2**, 1199–1208.
183 Y. Shen, J. Zhou, T. Liu, Y. Tao, R. Jiang, M. Liu, G. Xiao, J. Zhu, Z. K. Zhou, X. Wang, C. Jin and J. Wang, *Nat. Commun.*, 2013, **4**, 2381.
184 Z. Hu, Z. Liu, L. Li, B. Quan, Y. Li, J. Li and C. Gu, *Small*, 2014, **10**, 3933–3942.
185 N. G. Quilis, M. Lequeux, P. Venugopalan, I. Khan, W. Knoll, S. Boujday, M. L. de la Chapelle and J. Dostalek, *Nanoscale*, 2018, **10**, 10268–10276.
186 T. Andryszewski, M. Iwan, M. Hołdynski and M. Fia łkowski, *Chem. Mater.*, 2016, **28**, 5304–5313.
187 I. Šloufová-Srnová and B. Vlčkova, *Nano Lett.*, 2002, **2**, 121–125.
188 A. Li, S. K. Srivastava, I. Abdulhalim and S. Li, *Nanoscale*, 2016, **8**, 15658–15664.
189 M. Abutoama, S. Li and I. Abdulhalim, *J. Phys. Chem. C*, 2017, **121**, 27612–27623.
190 Y. Chu and K. h. B. Crozier, *Opt. Lett.*, 2009, **34**, 244–246.
191 M. Sarkar, M. Besbes, J. Moreau, J.-F. Bryche, A. Olivéro, G. Barbillon, A.-L. Coutrot, B. Bartenlian and M. Canva, *ACS Photonics*, 2015, **2**, 237–245.
192 H. X. a. D. Wang, *Adv. Mater.*, 2007, **20**, 4253–4256.
193 K. M. Mayer and J. H. Hafner, *Chem. Rev.*, 2011, **111**, 3828–3857.
194 C. Wang, Z. Ma, T. Wang and Z. Su, *Adv. Funct. Mater.*, 2006, **16**, 1673–1678.
195 S. Fayyaz, M. Tabatabaei, R. Hou and F. Lagugné-Labarthet, *J. Phys. Chem. C*, 2012, **116**, 11665–11670.
196 Z. Cai, Y. J. Liu, X. Lu and J. Teng, *J. Phys. Chem. C*, 2013, **117**, 9440–9445.
197 C. L. Zhang, K. P. Lv, H. P. Cong and S. H. Yu, *Small*, 2012, **8**, 647–653.
198 W. Cheng, M. J. Campolongo, J. J. Cha, S. J. Tan, C. C. Umbach, D. A. Muller and D. Luo, *Nat. Mater.*, 2009, **8**, 519–525.
199 Z. G. Estephan, Z. Qian, D. Lee, J. C. Crocker and S. J. Park, *Nano Lett.*, 2013, **13**, 4449–4455.
200 J. Gargiulo, T. Brick, I. L. Violi, F. C. Herrera, T. Shibanuma, P. Albella, F. G. Requejo, E. Cortes, S. A. Maier and F. D. Stefani, *Nano Lett.*, 2017, **17**, 5747–5755.
201 I. G. Theodorou, Z. A. R. Jawad, Q. Jiang, E. O. Aboagye, A. E. Porter, M. P. Ryan and F. Xie, *Chem. Mater.*, 2017, **29**, 6916–6926.
202 E. G. Matveeva, T. Shtoyko, I. Gryczynski, I. Akopova and Z. Gryczynski, *Chem. Phys. Lett.*, 2008, **454**, 85–90.
203 M. Tseng, M.-K. Hsiao, H. Huang, H. Chen, Y. Chen, C. Chu, N.-N. Chu, Y. He, C. Chang, W. Lin, D.-W. Huang, H.-P. Chiang, R.-S. Liu, G. Sun and D. P. Tsai, *ACS Nano*, 2012, **6**, 5190–5197.
204 A. Peer, Z. Hu, A. Singh, J. A. Hollingsworth, R. Biswas and H. Htoon, *Small*, 2017, **13**, 1700660.
205 B. Zhang, J. A. Jarrell, J. V. Price, S. M. Tabakman, Y. Li, M. Gong, G. Hong, J. Feng, P. J. Utz and H. Dai, *PLoS One*, 2013, **8**, e71043.
206 L. B. Zhong, J. Yin, Y. M. Zheng, Q. Liu, X. X. Cheng and F. H. Luo, *Anal. Chem.*, 2014, **86**, 6262–6267.
207 Q. Guo, M. Xu, Y. Yuan, R. Gu and J. Yao, *Langmuir*, 2016, **32**, 4530–4537.
208 E. Heydari, J. R. Sperling, S. L. Neale and A. W. Clark, *Adv. Funct. Mater.*, 2017, **27**, 1701866.
209 J. W. M. Chon, C. Bullen, P. Zijlstra and M. Gu, *Adv. Funct. Mater.*, 2007, **17**, 875–880.
210 J. Tang, Y. Wang, J. E. Klare, G. S. Tulevski, S. J. Wind and C. Nuckolls, *Angew. Chem., Int. Ed.*, 2007, **46**, 3892–3895.
211 H. Kang, C. J. Heo, H. C. Jeon, S. Y. Lee and S. M. Yang, *ACS Appl. Mater. Interfaces*, 2013, **5**, 4569–4574.
212 P. Anger, P. Bharadwaj and L. Novotny, *Phys. Rev. Lett.*, 2006, **96**, 113002.
213 L. Jiang, H. Mundoor, Q. Liu and I. I. Smalyukh, *ACS Nano*, 2016, **10**, 7064–7072.
214 Y. Yan, L. Meng, W. Zhang, Y. Zheng, S. Wang, B. Ren, Z. Yang and X. Yan, *ACS Sens.*, 2017, **2**, 1369–1376.
215 Z. Mei and L. Tang, *Anal. Chem.*, 2017, **89**, 633–639.
216 F. Xie, M. S. Baker and E. M. Goldy, *Chem. Mater.*, 2008, **20**, 1788–1797.
217 T. L. Jennings, M. P. Singh and G. F. Strouse, *J. Am. Chem. Soc.*, 2006, **128**, 5462–5467.
218 K. Aslan, I. Gryczynski, J. Malicka, E. Matveeva, J. R. Lakowicz and C. D. Geddes, *Curr. Opin. Biotechnol.*, 2005, **16**, 55–62.
219 S. M. Fothergill, C. Joyce and F. Xie, *Nanoscale*, 2018, **10**, 20914–20929.
220 N. A. Hatab, C. H. Hsueh, A. L. Gaddis, S. T. Retterer, J. H. Li, G. Eres, Z. Zhang and B. Gu, *Nano Lett.*, 2010, **10**, 4952–4955.
221 H. Chen and Y. Xia, *Anal. Chem.*, 2014, **86**, 11062–11069.
222 H. Li, J. Kang, J. Yang and B. Wu, *J. Phys. Chem. C*, 2016, **120**, 16907–16912.
223 M. R. B. Nardine, S. Abadeer, W. L. Wilson and C. J. Murphy, *ACS Nano*, 2014, **8**, 8392–8406.
224 F. Tang, N. Ma, X. Wang, F. He and L. Li, *J. Mater. Chem.*, 2011, **21**, 16943.
225 L. Lin, L. Liu, K. Musselman, G. Zou, W. W. Duley and Y. N. Zhou, *Adv. Funct. Mater.*, 2016, **26**, 5979–5986.
226 A. Kinkhabwala, Z. Yu, S. Fan, Y. Avlasevich, K. Müllen and W. E. Moerner, *Nat. Photonics*, 2009, **3**, 654–657.
227 H. Yuan, S. Khatua, P. Zijlstra, M. Yorulmaz and M. Orrit, *Angew. Chem., Int. Ed.*, 2013, **52**, 1217–1221.
228 R. Alvarez-Puebla, L. M. Liz-Marzán and F. J. García de Abajo, *J. Phys. Chem. Lett.*, 2010, **1**, 2428–2434.
229 J. F. Li, C. Y. Li and R. F. Aroca, *Chem. Soc. Rev.*, 2017, **46**, 3962–3979.
230 I. G. Theodorou, Z. A. Jawad, H. Qin, E. O. Aboagye, A. E. Porter, M. P. Ryan and F. Xie, *Nanoscale*, 2016, **8**, 12869–12873.

231 Z. Mei and L. Tang, *Anal. Chem.*, 2017, **89**, 633–639.
232 H. Ko, S. Singamaneni and V. V. Tsukruk, *Small*, 2008, **4**, 1576–1599.
233 B. N. Khlebtsov, V. A. Khanadeev, M. Y. Tsvetkov, V. N. Bagratashvili and N. G. Khlebtsov, *J. Phys. Chem. C*, 2013, **117**, 23162–23171.
234 V. Liberman, C. Yilmaz, T. M. Bloomstein, S. Somu, Y. Echegoyen, A. Busnaina, S. G. Cann, K. E. Krohn, M. F. Marchant and M. Rothschild, *Adv. Mater.*, 2010, **22**, 4298–4302.
235 A. Campion and P. Kambhampati, *Chem. Soc. Rev.*, 1998, **27**, 241.
236 J. F. Betz, W. W. Yu, Y. Cheng, I. M. White and G. W. Rubloff, *Phys. Chem. Chem. Phys.*, 2014, **16**, 2224–2239.
237 S. L. Kleinman, R. R. Frontiera, A. I. Henry, J. A. Dieringer and R. P. Van Duyne, *Phys. Chem. Chem. Phys.*, 2013, **15**, 21–36.
238 X. Y. L. Martin, J. Mulvihill, J. Henzie and P. Yang, *J. Am. Chem. Soc.*, 2010, **132**, 268–274.
239 Q. Li, Y. Jiang, R. Han, X. Zhong, S. Liu, Z. Y. Li, Y. Sha and D. Xu, *Small*, 2013, **9**, 927–932.
240 H. Dai, S. Chen, Y. Li, B. Zeng, S. Zhang, Z. Hong and Y. Lin, *Biosens. Bioelectron.*, 2017, **92**, 687–694.
241 X. Kong, Q. Yu, X. Zhang, X. Du, H. Gong and H. Jiang, *J. Mater. Chem.*, 2012, **22**, 7767.
242 B. Kokuoz, K. G. Kornev and I. Luzinov, *ACS Appl. Mater. Interfaces*, 2009, **1**, 575–583.
243 J. Hrabakova, K. Ataka, J. Heberle, P. Hildebrandt and D. H. Murgida, *Phys. Chem. Chem. Phys.*, 2006, **8**, 759–766.
244 W. Shen, X. Lin, C. Jiang, C. Li, H. Lin, J. Huang, S. Wang, G. Liu, X. Yan, Q. Zhong and B. Ren, *Angew. Chem., Int. Ed.*, 2015, **54**, 7308–7312.
245 X.-D. Lin, V. Uzayisenga, J.-F. Li, P.-P. Fang, D.-Y. Wu, B. Ren and Z.-Q. Tian, *J. Raman Spectrosc.*, 2012, **43**, 40–45.
246 X. Qiao, B. Su, C. Liu, Q. Song, D. Luo, G. Mo and T. Wang, *Adv. Mater.*, 2018, **30**, 1702275.
247 J.-W. Jeon, J. Zhou, J. A. Geldmeier, J. F. Ponder, M. A. Mahmoud, M. El-Sayed, J. R. Reynolds and V. V. Tsukruk, *Chem. Mater.*, 2016, **28**, 7551–7563.
248 M. L. Tseng, J. Yang, M. Semmlinger, C. Zhang, P. Nordlander and N. J. Halas, *Nano Lett.*, 2017, **17**, 6034–6039.
249 P. Guo, M. S. Weimer, J. D. Emery, B. T. Diroll, X. Chen, A. S. Hock, R. P. Chang, A. B. Martinson and R. D. Schaller, *ACS Nano*, 2017, **11**, 693–701.
250 S. L. Kathryn, M. Mayer, H. Liao, B. C. Rostro, A. Fuentes, P. T. Scully, C. L. Nehl and J. H. Hafner, *ACS Nano*, 2008, **2**, 687–692.
251 W. P. Hall, J. N. Anker, Y. Lin, J. Modica, M. Mrksich and R. P. Van Duyn, *J. Am. Chem. Soc.*, 2008, **130**, 5836–5837.
252 A. Emboras, J. Niegemann, P. Ma, C. Haffner, A. Pedersen, M. Luisier, C. Hafner, T. Schimmel and J. Leuthold, *Nano Lett.*, 2016, **16**, 709–714.
253 A. Dong, J. Chen, P. M. Vora, J. M. Kikkawa and C. B. Murray, *Nature*, 2010, **466**, 474–477.
254 N. Jiang, L. Shao and J. Wang, *Adv. Mater.*, 2014, **26**, 3282–3289.
255 M. L. Tseng, J. Yang, M. Semmlinger, C. Zhang, P. Nordlander and N. J. Halas, *Nano Lett.*, 2017, **17**, 6034–6039.
256 Z. Jiang, J. He, S. A. Deshmukh, P. Kanjanaboos, G. Kamath, Y. Wang, S. K. Sankaranarayanan, J. Wang, H. M. Jaeger and X. M. Lin, *Nat. Mater.*, 2015, **14**, 912–917.
257 J.-H. Huh, J. Lee and S. Lee, *ACS Photonics*, 2017, **5**, 413–421.
258 S. Christau, T. Moeller, J. Genzer, R. Koehler and R. von Klitzing, *Macromolecules*, 2017, **50**, 7333–7343.
259 Z. Qian and D. S. Ginger, *J. Am. Chem. Soc.*, 2017, **139**, 5266–5276.
260 L. Cheng, S. Peng and H. Duan, *ACS Nano*, 2010, **4**, 6098–6104.
261 L. Wang, J. Luo, J. Yin, H. Zhang, J. Wu, X. Shi, E. Crew, Z. Xu, Q. Rendeng, S. Lu, M. Poliks, B. Sammakia and C.-J. Zhong, *J. Mater. Chem.*, 2010, **20**, 907–915.
262 A. Abbas, M. J. Linman and Q. Cheng, *Biosens. Bioelectron.*, 2011, **26**, 1815–1824.
263 J.-E. Lee, K. Chung, J. Lee, K. Shin and D. H. Kim, *Adv. Funct. Mater.*, 2015, **25**, 6716–6724.
264 I. Luzinov, S. Minko and V. V. Tsukruk, *Soft Matter*, 2008, **4**, 714–725.
265 I. Tokareva, S. Minko, J. H. Fendler and E. Hutter, *J. Am. Chem. Soc.*, 2004, **126**, 15950–15951.
266 O. Graydon, *Nat. Photonics*, 2015, **9**, 487–488.
267 J. S. Clausen, E. Hojlund-Nielsen, A. B. Christiansen, S. Yazdi, M. Grajower, H. Taha, U. Levy, A. Kristensen and N. A. Mortensen, *Nano Lett.*, 2014, **14**, 4499–4504.
268 B. Liu, X. Lu, Z. Qiao, L. Song, Q. Cheng, J. Zhang, A. Zhang, Y. Huang and T. Chen, *Langmuir*, 2018, **34**, 13047–13056.
269 G. Wang, X. Chen, S. Liu, C. Wong and S. Chu, *ACS Nano*, 2016, **10**, 1788–1794.
270 M. Gu, X. Li and Y. Cao, *Light: Sci. Appl.*, 2014, **3**, e177–e177.
271 X. Ouyang, Y. Xu, Z. Feng, W. Tang, Y. Cao and X. Li, *Nanoscale*, 2019, **11**, 2447–2452.
272 Q. Zhang, Z. Xia, Y. B. Cheng and M. Gu, *Nat. Commun.*, 2018, **9**, 1183.
273 Q. Dai, M. Ouyang, W. Yuan, J. Li, B. Guo, S. Lan, S. Liu, Q. Zhang, G. Lu, S. Tie, H. Deng, Y. Xu and M. Gu, *Adv. Mater.*, 2017, **29**, 1701918.
274 L. Dai, X. Lu, L. Song, Y. Huang, B. Liu, L. Zhang, J. Zhang, S. Wu and T. Chen, *Adv. Mater. Interfaces*, 2018, **5**, 1800026.
275 Y. Chu, H. Xiao, G. Wang, J. Xiang, H. Fan, H. Liu, Z. Wei, S. Tie, S. Lan and Q. Dai, *J. Phys. Chem. C*, 2018, **122**, 15652–15658.
276 M. Gu, Q. Zhang and S. Lamon, *Nat. Rev. Mater.*, 2016, **12**, 16070.

277 P. Zijlstra, J. W. M. Chon and M. Gu, *Nature*, 2009, **459**, 410–413.
278 A. S. Roberts, S. M. Novikov, Y. Yang, Y. Chen, S. Boroviks, J. Beermann, N. A. Mortensen and S. I. Bozhevolnyi, *ACS Nano*, 2019, **13**, 71–77.
279 H. Wohltjen and A. W. Snow, *Anal. Chem.*, 1998, **70**, 2856–2859.
280 Z. Nie, D. Fava, M. Rubinstein and E. Kumacheva, *J. Am. Chem. Soc.*, 2008, **130**, 3683–3689.
281 Y. Wang, A. E. DePrince 3rd, S. K. Gray, X. M. Lin and M. Pelton, *J. Phys. Chem. Lett.*, 2010, **1**, 2692–2698.
282 N. Olichwer, A. Meyer, M. Yesilmen and T. Vossmeyer, *J. Mater. Chem. C*, 2016, **4**, 8214–8225.
283 W. P. Wuelfing, S. J. Green, J. J. Pietron, D. E. Cliffel and R. W. Murray, *J. Am. Chem. Soc.*, 2000, **122**, 11465–11472.
284 N. Olichwer, E. W. Leib, A. H. Halfar, A. Petrov and T. Vossmeyer, *ACS Appl. Mater. Interfaces*, 2012, **4**, 6151–6161.
285 E. García-Berríos, T. Gao, J. C. Theriot, M. D. Woodka, B. S. Brunschwig and N. S. Lewis, *J. Phys. Chem. C*, 2011, **115**, 6208–6217.
286 R. A. Potyrailo, M. Larsen and O. Riccobono, *Angew. Chem., Int. Ed.*, 2013, **52**, 10360–10364.
287 S. Shan, W. Zhao, J. Luo, J. Yin, J. C. Switzer, P. Joseph, S. Lu, M. Poliks and C.-J. Zhong, *J. Mater. Chem. C*, 2014, **2**, 1893.
288 N. Shehada, J. C. Cancilla, J. S. Torrecilla, E. S. Pariente, G. Bronstrup, S. Christiansen, D. W. Johnson, M. Leja, M. P. Davies, O. Liran, N. Peled and H. Haick, *ACS Nano*, 2016, **10**, 7047–7057.
289 Y. Y. Broza, P. Mochalski, V. Ruzsanyi, A. Amann and H. Haick, *Angew. Chem., Int. Ed.*, 2015, **54**, 11036–11048.
290 V. Ruzsanyi, W. Lederer, C. Seger, B. Calenic, K. R. Liedl and A. Amann, *J. Breath Res.*, 2014, **8**, 046005.
291 M. Segev-Bar and H. Haick, *ACS Nano*, 2013, **7**, 8366–8378.
292 T. P. Huynh and H. Haick, *Adv. Mater.*, 2016, **28**, 138–143.
293 H. H. Chou, A. Nguyen, A. Chortos, J. W. To, C. Lu, J. Mei, T. Kurosawa, W. G. Bae, J. B. Tok and Z. Bao, *Nat. Commun.*, 2015, **6**, 8011.
294 D. Son, J. Kang, O. Vardoulis, Y. Kim, N. Matsuhisa, J. Y. Oh, J. W. To, J. Mun, T. Katsumata, Y. Liu, A. F. McGuire, M. Krason, F. Molina-Lopez, J. Ham, U. Kraft, Y. Lee, Y. Yun, J. B. Tok and Z. Bao, *Nat. Nanotechnol.*, 2018, **13**, 1057–1065.
295 S. Park, H. Kim, M. Vosgueritchian, S. Cheon, H. Kim, J. H. Koo, T. R. Kim, S. Lee, G. Schwartz, H. Chang and Z. Bao, *Adv. Mater.*, 2014, **26**, 7324–7332.
296 C. Pang, G. Y. Lee, T. I. Kim, S. M. Kim, H. N. Kim, S. H. Ahn and K. Y. Suh, *Nat. Mater.*, 2012, **11**, 795–801.
297 S. Wang, J. Xu, W. Wang, G. N. Wang, R. Rastak, F. Molina-Lopez, J. W. Chung, S. Niu, V. R. Feig, J. Lopez, T. Lei, S. K. Kwon, Y. Kim, A. M. Foudeh, A. Ehrlich, A. Gasperini, Y. Yun, B. Murmann, J. B. Tok and Z. Bao, *Nature*, 2018, **555**, 83–88.
298 M. P. R. William, H. Steinecker and E. T. Zellers, *Anal. Chem.*, 2007, **79**, 4977–4986.
299 H. Feng, Y. Yang, Y. You, G. Li, J. Guo, T. Yu, Z. Shen, T. Wu and B. Xing, *Chem. Commun.*, 2009, 1984–1986, DOI: 10.1039/b822507a.
300 Z. Huo, C. K. Tsung, W. Huang, X. Zhang and P. Yang, *Nano Lett.*, 2008, **8**, 2041–2044.
301 B. Zhu, S. Gong, F. Lin, Y. Wang, Y. Ling, T. An and W. Cheng, *Adv. Electron. Mater.*, 2019, **5**, 1800509.
302 Q. Zhai, Y. Wang, S. Gong, Y. Ling, L. W. Yap, Y. Liu, J. Wang, G. P. Simon and W. Cheng, *Anal. Chem.*, 2018, **90**, 13498–13505.
303 L. Pan, A. Chortos, G. Yu, Y. Wang, S. Isaacson, R. Allen, Y. Shi, R. Dauskardt and Z. Bao, *Nat. Commun.*, 2014, **5**, 3002.
304 M.-j. Yin, Y. Zhang, Z. Yin, Q. Zheng and A. P. Zhang, *Adv. Mater. Technol.*, 2018, **3**, 1800051.

